Precursor molecules for cobalt(II) single molecule magnets – Synthesis and magnetic properties

David Hunger[‖,‡] *, Simon Suhr*[⊥,‡]*, Valentin Bayer*[‖]*, Uta Albold*[§]*, Biprajit Sarkar*[⊥,*]*, Joris van Slageren*[‖,*]

[‖] Institut für Physikalische Chemie, Universität Stuttgart, Pfaffenwaldring 55, 70569 Stuttgart, Germany

[⊥] Institut für Anorganische Chemie, Universität Stuttgart, Pfaffenwaldring 55, 70569 Stuttgart, Germany

[§] Institut für Chemie und Biochemie, Freie Universität Berlin, Fabeckstraße 34-36, 14195 Berlin, Germany

[‡] Equal Contribution

KEYWORDS: 3d metals, magnetism, single-molecule magnets, SQUID magnetometry, HF-EPR spectroscopy

ABSTRACT

Molecular magnetic materials based on 1,2-diamidobenzenes are well known and have been intensively studied both experimentally and computationally. They feature interesting magnetic properties as well as redox activity. In this work, we present the synthesis and investigation of potent synthons for constructing discrete metal-organic architectures featuring 1,2-diamidobenzene-coordinated metal centers. The synthons feature weakly bound dimethoxyethane (DME) ligands in addition to the 1,2-diamidobenzene. We characterize these complexes and investigate their magnetic properties by means of static and dynamic magnetometry and high-field electron paramagnetic resonance (HFEPR). Interestingly, the magnetic and magnetic resonance data strongly suggest a dimeric formulation of these complexes, viz. $[M(II)(bmsab)DME]_2$ (bmsab = 1,2-bis(methanesulfonamido)benzene) with M = Co, Ni, Zn. This formulation is supported by ab initio calculations. A large negative *D*-value of −60 cm^{-1} was found for the Co(II) synthon and an equally large negative *D* of -50 cm^{-1} for the Ni(II) synthon. For Co(II), this *D*-value is in line to what was found for the known bis-diamidobenzene complexes of this ion. In contrast, the negative *D*-value for the nickel(II) complex is inexpected, which we explain in terms of increased effective coordination numbers. In contrast to the homoleptic Co(II) 1,2-diamidobenzene complex, the heteroleptic Co(II) complex presented here does not feature slow relaxation of the magnetization.

INTRODUCTION

Single-molecule magnets (SMMs) offer the possibility to store data on a molecular level, which would allow a much higher storage density than currently possible. Careful ligand field design can induce strong magnetic anisotropy due to zero-field splitting (ZFS) in transition metal complexes, which is a prerequisite for SMM behavior. Compounds of 1,2-bis(sulfonamido)benzenes have

been shown to be excellent ligands for engendering very large ZFS *D*-values in various metal centers due to their acute bite angle, which leads to a strong axial distortion. For diamidobenzene complexes of cobalt(II) very large negative *D*-values were found, making these complexes excellent SMM candidates.[1,2,3,4] Related nickel(II) complexes exhibit large positive *D* values (in the region of 60 cm^{-1}).[2] The investigations of various ligand systems based on 1,2-diamidobenzenes showed that the magnetic properties of especially cobalt(II) complexes of these ligands are very robust and the large ZFS is conserved also with different sulfonamido donors. The strongly electron-withdrawing nature of the sulfonamido substituents provides an additional advantage, as it stabilizes the anionic complexes and makes them stable towards air and moisture. This is a beneficial aspect with respect to possible future applications. Despite the strong anisotropy, true magnetic bistability was not observed in transition metal complexes of 1,2-diamidobenzenes, due to efficient under-barrier relaxation. An approach to overcoming this challenge lies in developing polynuclear metal complexes, where the spin centers are strongly coupled. The energy scale of the coupling must be at least that of the ZFS to prevent giving rise to low-lying spin-excited states that facilitate magnetic relaxation. In practice, this means using radical bridging ligands.[6,7,8,9] Along these lines, our groups recently presented a binuclear, radical bridged cobalt(II) complex based on similar ligands[5], which displays superior magnetic relaxation properties compared to its mononuclear counterpart. However, the synthetic procedure for obtaining this compound was not convenient, and the desired product could only be obtained in low yields by manual sorting of crystals. Hence a rational and modular approach to such compounds necessitates novel precursors, in which precisely one 1,2-diamidobenzene ligand is firmly bound to the central metal, while the coordination sphere is completed by labile co-ligands. Such novel synthons would open ways to develop multinuclear systems and other heteroleptic

complexes of 1,2-diamidobenzenes. This approach (among others) was reviewed by Pedersen, Bendix and Clérac in 2014,[10] and is illustrated in Scheme 1 for the present case. In this work, the synthetic route as well as an in depth magnetic characterization of the heteroleptic complexes of the composition [M(II)(bmsab)DME] is presented (DME = dimethoxyethane, M = Co, Ni, Zn).

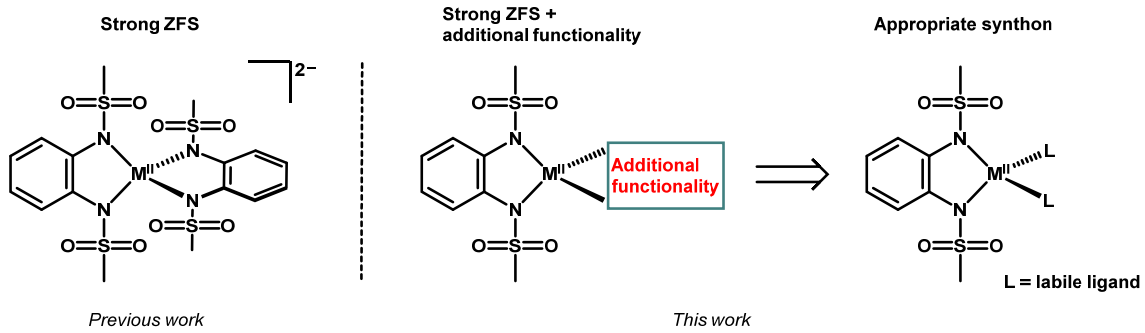

Scheme 1. Conceptual approach: a modular route to functional heteroleptic structures requires appropriate synthons.

SYNTHESIS AND CHARACTERIZATION

Our synthetic route is based on previous work by Khusniyarov and Wieghardt who reported the synthesis of an extremely air-sensitive six-coordinate heteroleptic 1,2-diamidobenzene Fe(II) complex from a diamido iron(II) precursor and 1,2-diamidobenzene as the limiting reagent.[11] Similarly, we used divalent amides of the respective metals as starting materials for the synthesis of the three complexes [Zn(II)(bmsab)DME] (**1**), [Ni(II)(bmsab)DME] (**2**) and [Co(II)(bmsab)DME] (**3**), since they are readily accessible and provide a strong internal base in the correct stoichiometry. In the case of Co(II) and Zn(II), the well-known hexamethyldisilazides were used.[12] For the corresponding Ni(II) complex, the hexamethyldisilazide was recently reported as its THF adduct [13], however, this is a rather unsuitable starting material, due to its thermal instability[14]. Instead, for **2**, the divalent Ni(II) amide Ni[N(SiMe$_3$)(DIPP)]$_2$ (DIPP = diisopropyphenyl) as described by Tilley et al.[15] was chosen as a starting material. The heteroleptic metal complexes were then obtained by dropwise addition of a solution of the metal amide in DME

(for Co(II) and Zn(II)) or toluene (Ni(II)) to a cooled (−20°C) suspension of H_2bmsab in DME (see Scheme 2). After warming to room temperature, the products were precipitated by addition of hexane. After filtration and drying under high vacuum, pink (Co(II)), red (Ni(II)) or colorless (Zn(II)) amorphous powders are isolated. The complexes themselves are air- and moisture-sensitive and insoluble in all common solvents, apart from acetonitrile. Dissolving into acetonitrile leads to a ligand exchange reaction, which can be followed by ^{1}H NMR spectroscopy (*vide infra*). Consequently, characterization is demanding, but elemental analysis is consistent with a formulation where each compound contains one dianionic $(bmsab)^{2-}$ and one molecule of DME per metal ion. This suggests the presence of four-coordinate metal centers. Magnetochemical and theoretical investigations (*vide infra*) points towards dimeric structures in the solid state for the nickel(II) and cobalt(II) complexes **2** and **3**.

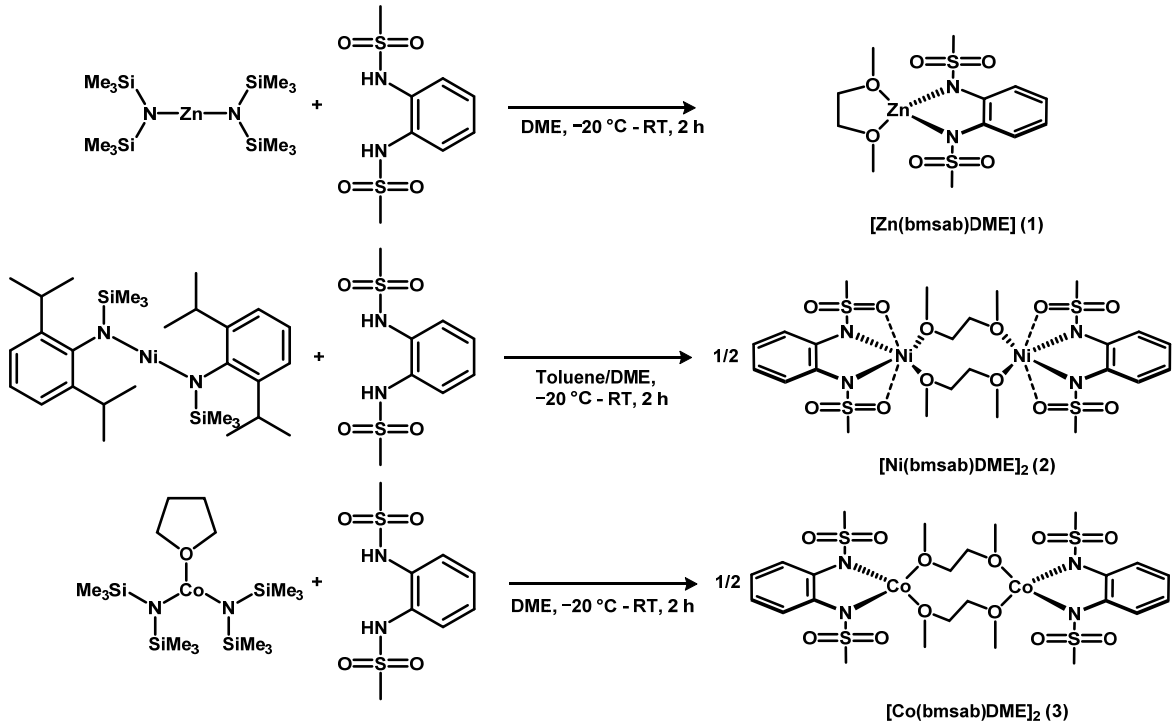

Scheme 2. Synthetic route towards the heteroleptic precursor compounds. Magnetometric measurements and calculations indicate a dimeric structure for **2** and **3**.

The identity of the compounds in solution was elucidated by means of (paramagnetic) ^{1}H NMR spectroscopy. The structurally well characterized homoleptic compounds[2] served as a reference. All spectra were recorded in deutero-acetonitrile. The most straightforward case is **1**, since Zn(II) is diamagnetic and hence the characterization by ^{1}H NMR is rather straightforward (see Supporting Information Figure S1). Three NMR resonances were found at δ = 7.26 (m, 2 H, bmsab-*H*-3,6), 6.73 (m, 2 H, bmsab-*H*-4,5), and 2.89 (s, 6 H, SO_2Me) ppm, which are similar to those observed for the homoleptic $[Zn(II)(bmsab)_2]^{2-}$ (7.36, 6.61, and 2.83 ppm, see Supporting Information Figure S2). Further resonances are observed at 3.45 and 3.28 ppm, which can be assigned to free DME, which points to the exchange of the weakly bound DME by acetonitrile. Similar behavior is found for **2**, where signals at 3.45 and 3.28 ppm point again to free DME. The resonance lines for [Ni(II)(bmsab)(DME)] are found at δ = 26.24 (6 H), 5.41 (2 H) and −5.27 (2 H) ppm and are almost identical to the homoleptic compound (albeit broadened), indicating that the coordination geometry in the dissolved complex **2** and the homoleptic counterpart are comparable (Supporting Information Figures S3 and S4). This is supported by UV/Vis/NIR measurements. A solution of **2** in acetonitrile shows bands at 400 and 540 nm (figure S7). These features are very similar to those observed for the homoleptic complex in acetonitrile solution (Figure S8, Table S1). In contrast, complex **3** shows different behavior: While the heteroleptic cobalt(II) complex **3** displays resonances in a range of 35 ppm (Supporting Information Figure S5), the homoleptic analog features NMR resonances that span a range of about 150 ppm (Supporting Information Figure S6). This indicates a different coordination environment of **3** in acetonitrile. UV/Vis/NIR spectra of an acetonitrile solution of **3** showed bands at 405 nm and 1120 nm (Supporting Information Figure

S9) that are not found in the homoleptic analog (Table S1). These bands can be tentatively assigned to the $^4T_{2g} \leftarrow {}^4T_{1g}$ and the $^4T_{1g}(P) \leftarrow {}^4T_{1g}$ transitions of an octahedrally coordinated high-spin d^7 system.[16] Hence, we propose that upon dissolution in acetonitrile, the labile DME ligands are replaced by four solvent molecules per Co(II) center to give a pseudo-octahedral coordination geometry. While the facile ligand exchange hampers the characterization of the DME adducts in solution, this exchange process indicates that we successfully isolated a suitable precursor with a labile co-ligand, which allows the stepwise building of heteroleptic, potentially polynuclear coordination compounds.

MAGNETISM AND EPR SPECTROSCOPY

A thorough magnetic characterization was performed to further characterize the heteroleptic species. For **3**, a room temperature χT value of 3.33 $cm^3\,K\,mol^{-1}$ is found, which is the value expected for a high spin Co(II) center ($S = 3/2$) with $g_{iso} = 2.66$. Upon cooling, χT decreases gradually until 12 K, which indicates a significant ZFS. On further cooling below 12 K, a steep drop in χT is observed. This drop cannot be simulated considering a large ZFS alone (see below), but must be due to other phenomena such as intramolecular antiferromagnetic interactions or slow dynamics of the magnetic moment. Simulations of the magnetic data were carried out based on the spin Hamiltonian in eq. (1).

$$H = \sum_{i=1}^{2}\left(g_i \vec{B}\mu_B \widehat{\boldsymbol{S}}_i + D_i \widehat{\boldsymbol{S}}_{z,i}^2 + E_i\left(\widehat{\boldsymbol{S}}_{x,i}^2 - \widehat{\boldsymbol{S}}_{y,i}^2\right)\right) + J\widehat{\boldsymbol{S}}_1^T\widehat{\boldsymbol{S}}_2 \quad (1)$$

Here, $J\widehat{\boldsymbol{S}}_1^T\widehat{\boldsymbol{S}}_2$ is the isotropic exchange interaction term, while the other terms describe the Zeeman, and the axial, and rhombic zero-field splittings, respectively. A good agreement of the experimental susceptibility temperature product with the simulated one is obtained considering two $S = 3/2$ centers with $g_{iso} = 2.68(5)$, $D = -60(5)\ cm^{-1}$, $E = 0$ and $J = 0.25(3)\ cm^{-1}$.

Hence, the simulation indicates that a non-negligible exchange interaction is present. This is evident when comparing simulations with and without such an interaction (Figure 1). Magnetization curves at different temperatures can be simulated in good accordance with the experiment based on a slightly larger g-value of $g_{\mathrm{iso}} = 2.75(3)$ and a slightly larger exchange interaction of $J = 0.30(3)\ \mathrm{cm}^{-1}$ (Supporting Information Figure S10).

On the basis of the elemental analysis data and the magnetometry, it is already possible to obtain insight into the molecular structure of **3** in the solid state. Since the elemental analysis is in good accordance with one DME and one bmsab ligand for one Co(II) center, the smallest structure that can feature some intramolecular exchange interaction is a dimer, with two bridging DME ligands between two Co(II)(bmsab) moieties. Similar bridging structures have been reported for the Co(II)(bmsab) fragment in 2022 by Shao et. al.[29] Further proof of such a structural motif was obtained by means of HFEPR spectroscopy (see below).

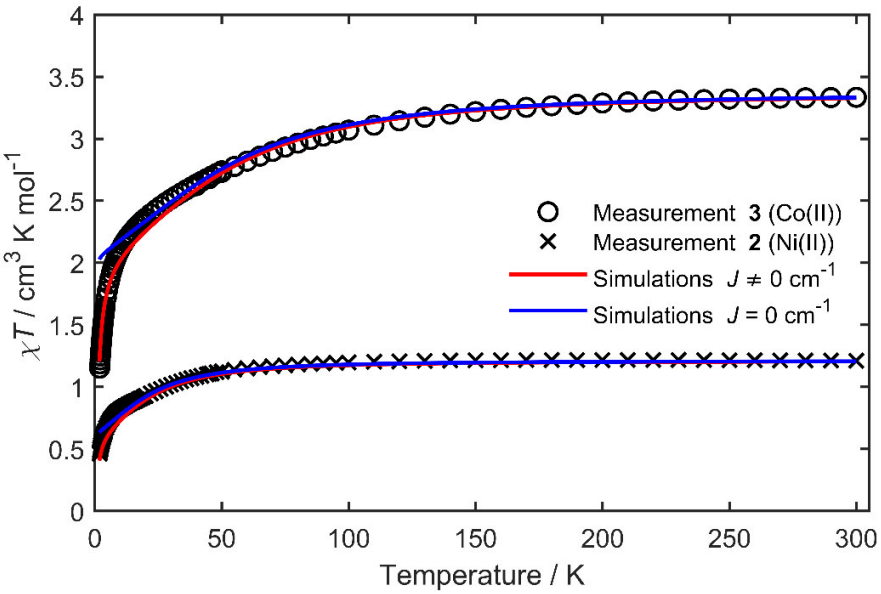

Figure 1. Susceptibility temperature product of **2** and **3** as a function of the temperature (black symbols) recorded on pressed powder samples at external fields of 0.1 T ($T < 40$ K) and at 1 T ($T > 40$ K). Lines are fits according to Eq. (1). The parameters are given in Table 1.

Due to the pronounced negative zero-field splitting, **3** is expected to be EPR-silent at X-band frequencies (9.5 GHz): A large negative D leads to a substantial energetic separation between the Kramers doublets and renders the $m_S = \pm 3/2$ doublet the ground state.[17] The intradoublet transition within the $m_S = \pm 3/2$ doublet is EPR-forbidden. Indeed, powder EPR experiments on **3** at 9.5 GHz yield no signal over a temperature range of 4.5 K to 300 K. In contrast, a frozen solution of **3** in acetonitrile gives an intense, broadened signal at 4.5 K with effective g-values of 4.99, 3.69 and 2.92, when using an $S_{\text{eff}} = 1/2$ model (see Figure 2). These values are in good accordance with literature known effective g-values for octahedral Co(II) complexes and are hence indicative for a formation of an octahedrally coordinated high-spin Co(II) species of **3** in acetonitrile.[32,33] This is a further confirmation for the ligand exchange reaction described above.

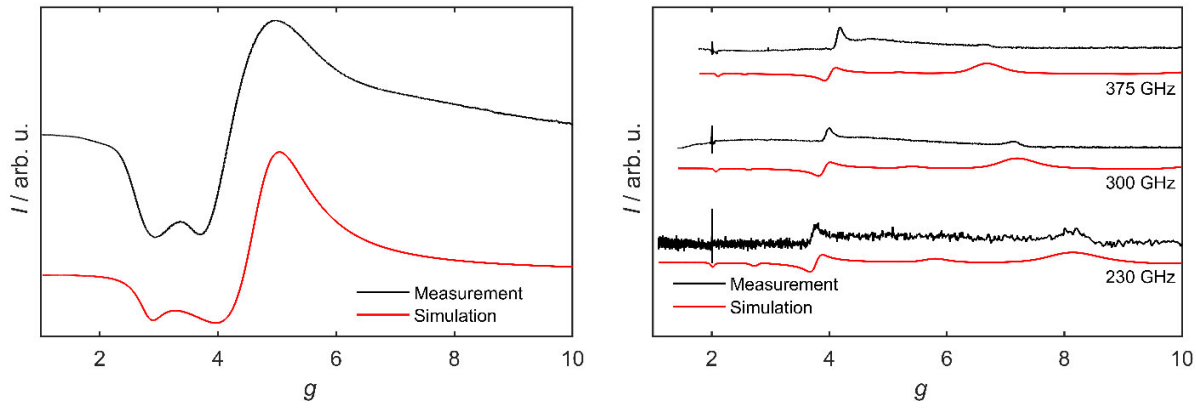

Figure 2. Left: Experimental X-band EPR spectrum of an acetonitrile solution of **3** at 4 K, and a simulation considering a a pseudo $S = 1/2$ system. Right: HFEPR spectra of **3** as a pressed powder at 230, 300 and 375 GHz, in magnetic fields of up to 15 T and at 5 K (black). The

corresponding HFEPR simulation based on two interacting pseudo $S = 1/2$ systems is shown in red.

To gain additional insight into the electronic structure of **3**, high-field electron paramagnetic resonance (HFEPR) spectra were recorded at frequencies of up to 375 GHz on the same sample which was used for magnetometry. HFEPR measurements of samples of **3** gave reasonably well resolved spectra at 230, 300 and 375 GHz at a temperature of 5 K. Three main experimental features are observed in the 375 GHz measurement: Sharp signals at fields of 12.76 T ($g_{\mathrm{eff}} = 2.1$) and 6.38 T ($g_{\mathrm{eff}} = 4.2$) as well as a broader feature at 3.99 T ($g_{\mathrm{eff}} = 6.7$). The sharp signal at $g_{\mathrm{eff}} = 2.0$ is due to an impurity in the experimental setup. For a direct comparison of the spectra of **3** at various frequencies, it is useful to plot the spectra on a *g*-value scale. Here, a frequency dependency of the effective *g*-values is observed: The sharp signal at $g_{\mathrm{eff}} = 2.1$ (375 GHz) and the central feature at $g_{\mathrm{eff}} = 4.2$ (375 GHz) trend to lower *g*-values with decreasing frequency, while their spacing is also gradually decreasing (from 2.10 down to 1.81). The broad feature at $g_{\mathrm{eff}} = 6.7$ (375 GHz) moves to higher effective *g*-values at the lower frequencies ($g_{\mathrm{eff}} = 8.2$ at 230 GHz). These shifts must be due to a field-independent interaction. A first approach to modelling the HFEPR data is a description featuring two interacting pseudo $S = 1/2$ systems. This approach is valid due to the large ZFS of **3**, which results in a strongly isolated ground Kramers doublet. For this approach, effective *g*-values are used. An adequate simulation (see figure 2) of the frequency dependency of the signals at low *g*-values in the HFEPR spectra at 230, 300 and 375 GHz is obtained by using effective *g*-values of $g_{\mathrm{x}\prime} = 2.30(3)$, $g_{y\prime} = 4.50(5)$, $g_{\mathrm{z}\prime} = 5.20(5)$. The frequency dependence of the *g*-values is taken into account by an anisotropic exchange interaction of $J_{x,y,z} = (5.5(2), 6.0(1), 0.2(2))$ cm^{-1}.

In the description with two pseudo $S = 1/2$ systems, the anisotropy of each magnetic center is projected onto the exchange interaction. To expand the description of the HFEPR measurements and to obtain more in-depth insight in the spin system of **3**, especially in the coupling situation, a second modelling approach was implemented, which features two coupled $S = 3/2$ centers. The largest agreement of the simulations based on eq. (1) with the HFEPR experiments is obtained with parameters of (for each $S = 3/2$ center) $g_{x,y} = 2.25(3)$, $g_z = 2.30(5)$, $D = -60(10)$ cm^{-1}, $E = 0.1D$ and $J = 0.50(5)$ cm^{-1}. Even though the experiment is not perfectly reproduced, all the main experimentally observed features can be reproduced in the correct intensity ratio, and with the right frequency dependence by the simulation. On the basis of the simulations, the most interesting signal in the HFEPR spectra is the one at high g-values that shows the largest g-value shift with frequency. The distance of this signal to the signal at low g-values is sensitive towards the magnitude of J and hence allows a rather accurate determination of the exchange strength. The g-values are lower ($g_{iso} = 2.26$) than the ones found by means of magnetometry ($g_{iso} = 2.68$). Such discrepancies can be attributed to weighing errors that occur in the process of the sample preparation of the magnetometry sample. The rhombicity ($E = 0.1D$) is larger than the value found by simulating the temperature dependence of the susceptibility-temperature product, where it was set to zero, which is due to the fact that magnetometry measurements are not very sensitive to E. In the HFEPR simulations, a sizeable E is needed in order to allow some transitions. Simulations based on the magnetometry parameters do not show any signals in the region of the experimental signals (Supporting Information Figure S11). The exchange interaction found by means of HFEPR is in good agreement with the findings from the magnetization measurements, and highlights that exchange interactions, rather than slow

relaxation of the magnetization, are responsible for the drop of χT at low temperatures. With this, the assumed dimer model is further supported by the HFEPR analysis.

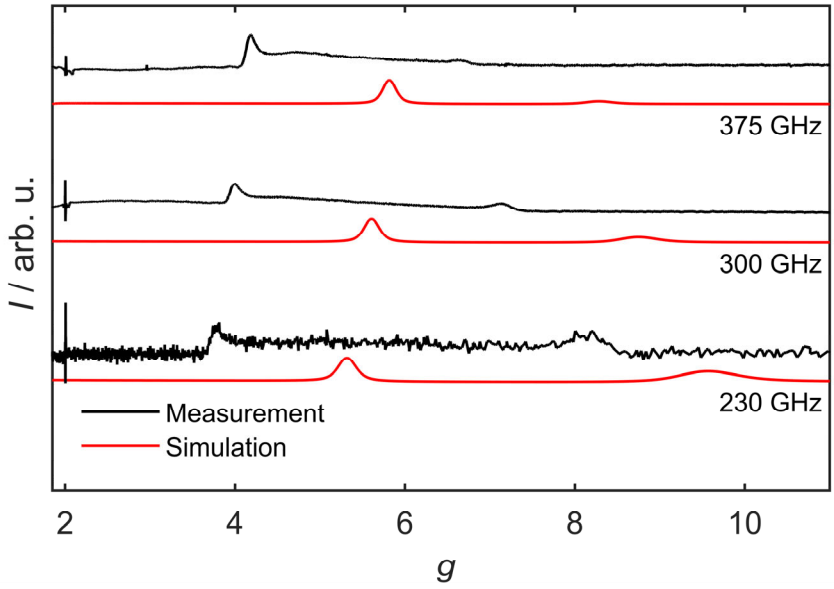

Figure 3. Measured HFEPR spectra of **3** at the indicated frequencies at 5 K (black). Simulations are shown in red. Simulations are based on two interacting $S = 3/2$ systems using the parameters given in the text.

Since the homoleptic analog of **3** ($[Co(bmsab)_2]^{2-}$) shows exceptional magnetic relaxation behavior, AC susceptibility measurements were carried out on **3**.[1,2] In these measurements, only a minor out-of-phase signal (χ''), that features two distinct peaks, is observed. The magnitude of this out-of-phase component is only 3 % of the in-phase component χ' of the dynamic susceptibility, Hence, only a minor fraction of the sample relaxes slowly, which is attributed to a small impurity, potentially of the homoleptic bis-bmsab complex (Supporting Information Figures S12 and S13). Hence, even though the heteroleptic DME complex **3** features a large, negative ZFS, it does not show signs of slow relaxation of the magnetization. This underlines how important the details of

the coordination environment are for the magnetic properties of molecules and their relaxation behavior.

In the case of **2**, the room temperature χT value is with 1.20 cm^3 K mol^{-1} in good agreement with $g_{iso} = 2.19$ and the d^8 configuration of Ni(II) (S =1). Upon decreasing temperature, χT is nearly constant down to 100 K, while on further temperature decrease, it decreases slightly to a value of 1.10 cm^3 K mol^{-1} at 50 K. Upon further cooling from 50 K to 1.8 K, χT decreases faster with decreasing temperature until it reaches 0.46 cm^3 K mol^{-1} at 1.8 K. This hints again to a rather large ZFS or a large exchange interaction also in the case of **2**. To quantify this, spin Hamiltonian simulations were carried out under a first assumption of a large and positive D, based on the parameters of the homoleptic $[Ni(II)(bmsab)_2]^{2-}$.[2] The best fit based on eq. (1) with respect of keeping the sign of D positive gave a parameter set for **2** with $g_{x,y,pos} = 2.10(2)$, $g_{z,pos} = 2.64(5)$, $D_{pos} = 35(5)\ cm^{-1}$ and $E_{pos} = D/3$. The exchange interaction strength was determined more precisely, by using the magnetization measurements and was found to be $J_{x,y,z,pos} = (10(2), -8(1), 16(3))\ cm^{-1}$. Nevertheless, the temperature dependence of χT and the magnetization curves are not well-reproduced (Supporting Information Figures S14 and S15) and the large anisotropy of the exchange tensor is rather unconvincing. Consequently, we removed the constraint of positive D for **2**. With this approach, an adequate agreement of experimental data and simulation was obtained with parameters of $g_{iso,neg} = 2.20(3)$, $D_{neg} = -50(5)\ cm^{-1}$, $E_{neg} = 0$ and $J_{iso,pos} = 0.5(1)\ cm^{-1}$ (Table 1). The magnetization curves were successfully simulated using the same parameters, with the additional inclusion of a small nonzero E-value of E/D = 0.04 (Supporting Information Figure S16). Even though a large, but negative D was not a priori expected in **2**, negative axial ZFS values have been reported for Ni(II) for higher coordination numbers than four, e.g., in octahedral geometries.[35-40] Hence, one alternate geometry might be a

pseudo octahedral geometry, where the sulfonyl oxygens saturate the coordination sphere around the Ni(II) centers. As mentioned above, large, negative ZFS *D*-values, exceeding $-20\ \mathrm{cm}^{-1}$ for octahedral or square bipyramidal Ni(II) are known in literature.[35-40]

Table 1: Overview over the spin Hamiltonian parameters for **2** and **3**. In the case of **2**, two parameter sets, either with a positive or a negative *D* are found (see text). In the context of this table, only the best-fit parameters are shown.

	[Co(II)(bmsab)DME]$_2$ (**3**)				[Ni(II)(bmsab)DME]$_2$ (**2**)			
	g	D/cm^{-1}	E/D	J/cm^{-1}	g	D/cm^{-1}	E/D	$J_{\mathrm{x,y,z}}/\mathrm{cm}^{-1}$
HFEPR	$g_{\mathrm{x,y}} = 2.25(3)$ $g_{\mathrm{z}} = 2.30(5)$	-60(10)	0.1	0.50(5)	–	–	–	–
χT vs. T	2.68(5)	-60(5)	0	0.25(3)	2.20(3)	-50(5)	0	$J_{\mathrm{iso}} = 0.5(1)$
M vs. H	2.75(3)	-60(5)	0	0.30(3)	2.20(3)	-50(5)	0.04	$J_{\mathrm{iso}} = 0.5(1)$
CASSCF	$g_{\mathrm{x},1} = 2.16$ $g_{\mathrm{y},1} = 2.18$ $g_{\mathrm{z},1} = 2.58$ $g_{\mathrm{x},2} = 2.17$ $g_{\mathrm{y},2} = 2.20$ $g_{\mathrm{z},2} = 2.55$	–34.5 –30.2	0.003 0.025	–	$g_{\mathrm{x},1} = 2.22$ $g_{\mathrm{y},1} = 2.27$ $g_{\mathrm{z},1} = 2.33$ $g_{\mathrm{x},2} = 2.23$ $g_{\mathrm{y},2} = 2.24$ $g_{\mathrm{z},2} = 2.30$	–10.66 –9.29	0.28 0.06	–

QUANTUM CHEMICAL CALCULATIONS

Because no single crystals suitable for x-ray diffraction could be obtained, the direct determination of the molecular structure was not possible. Therefore, a quantum chemical calculations of the electronic structure and the magnetic properties can complement the experimental findings. On the basis of the experimentally obtained structure of the homoleptic [M(II)(bmsab)$_2$]$^{2-}$ complexes[2] we constructed dimeric starting geometries for **2** and **3**, each featuring two bridging DME ligands between the two M(II) centers. The geometries were then optimized by DFT calculations (PBE0, def2-TZVP). In the case of **3**, the geometry optimization (Supporting Information Table S2, Figure S16) on DFT level resulted in a comparable geometry around the Co(II) centers to those found experimentally for other Co(II)bmsab adducts.[1,2] This can be highlighted, when the different Co-

N and intraligand C-N distances of **3** are compared to the experimental ones of the homoleptic complexes. Here, similar values are found and hence the theoretical structure of **3** is in good agreement with the expected bond lengths in the $bmsab^{2-}$ ligand (Supporting Information Table S6). Since the N-Co(II)-N bond angle of the ligands to the metal center strongly influences the ZFS[30], it is of great interest to compare this for **3** with experimentally found values for the homoleptic cases, where this bite angle ranges from 79.97 to 81.36°.[2] In the optimized structure of the heteroleptic complex **3**, values of 81.33 and 81.55° are found. This leads to the conclusion, that the binding geometry at the $bmsab^{2-}$ side in **3** matches the one in the homoleptic complex. For the O-Co(II)-O angles, angles of 106.34° or 110.21° are calculated for each one of the centers, i.e. much larger than the N-Co-N angle. Hence only one ligand-metal-ligand angle is highly acute and this is expected to lead to a decrease in axial ZFS.

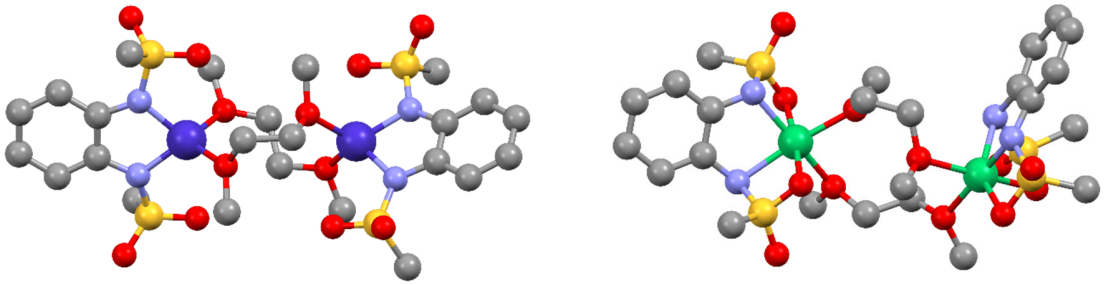

Figure 5. DFT optimized geometries of possible DME bridged dimers for the case of **2** and **3**. Cobalt ions are shown in dark blue, Nickel ions in green, oxygen in red, sulfur in yellow, nitrogen in light blue and carbon in grey. Hydrogens are omitted for clarity.

Since for the Ni(II) complex **2**, the magnetometry results suggest an octahedral or pseudo-octahedral geometry, a six-coordinate geometry around each Ni(II) center was assumed in the starting geometry for the DFT geometry optimization. This is justified by experimental data a number of structurally characterized Ni(II) complexes where sulfonamido groups act as bidentate

donors via N,O coordination.[44-46] Starting from a six-coordinate geometry in which the sulfonyl oxygen atoms act as axial donors, an optimum geometry was found (Table S3). Consequently, the geometry around the Ni(II) center is a slightly distorted octahedron. The bond distances between the Ni(II) centers and the bmsab^{2-} ligands range from 1.957 Å up to 2.223 Å, while the distances between the metal centers and the DME donors lie between 2.089 and 2.126 Å. The calculated distances between the two Ni(II) centers and the sulfonyl oxygens lie between 2.096 Å and 2.224 Å. Reported values of this structurally motif are in the range of 2.09[44] to 2.43 Å[46], hence the computations are in line with experimental precedence.

In order to calculate the magnetic properties of theoretical dimer structures and compare these with the experimental data, CAS(7,5) (Co(II)) or CAS(8,5) (Ni(II)) (def2-TZVPP for Co/Ni, N, O and def2-SVP for other elements) calculations were carried out to obtain values for the *g*-tensor and as well as parameters for the ZFS. Electron correlation was modeled on the NEVPT2 level. For these calculations, one of the Co(II) or Ni(II) centers were substituted by a diamagnetic Zn(II), while the geometry was unchanged. An effective Hamiltonian analysis of the projected relativistic states then allows access to the *g*-tensor and the ZFS parameters. These were found to be $g_{\mathrm{x}} = 2.16$, $g_y = 2.18$, $g_{\mathrm{z}} = 2.58$, $D = -34.5\ \mathrm{cm}^{-1}$, $E = |0.003D|$ in the case of Co(II) for one center (Table 1). For the second center, nearly similar *g*-values ($g_{\mathrm{x}} = 2.17, g_y = 2.20, g_z = 2.55$), but marginally different ZFS parameters of $D = -30.2\ \mathrm{cm}^{-1}$ and $E = |0.025D|$ were found, making the two spin-systems almost identical. This agrees with the comparable coordination geometry of both. For both centers, the first excited quartet state is the major contributor to the ZFS *D*-parameter (Supporting Information Tables S7 and S8). Good agreement is observed between the ab initio calculated values and the experimentally found spin Hamiltonian parameters in the case of **3** (Table 1) The calculated ZFS parameter *D* is nearly identical to the one obtained from

experiments. For the *g*-values, smaller numbers are calculated, but the *g*-tensor anisotropy is also axial.

In the Ni(II) case, values of $g_{\mathrm{x}} = 2.22$, $g_y = 2.27$, $g_{\mathrm{z}} = 2.33$, $D = -10.66\ \mathrm{cm}^{-1}$, $E = |0.28D|$ were calculated for Ni1 (Table 1). For Ni2, $g_{\mathrm{x}} = 2.23, g_y = 2.24, g_z = 2.30$, $D = -9.29\ \mathrm{cm}^{-1}$ and $E = |0.06D|$ are found. For both Ni(II) centers, the same magnitude for *D* and also a negative sign is found, being in line with the experimental findings. In the case of **2**, it was observed that for both centers the first three triplet states play a major role for the magnitude of the ZFS *D* parameter (Supporting Information Tables S9 and S10). For Ni1, $g_{\mathrm{iso}} = 2.27$ and for Ni2 $g_{\mathrm{iso}} = 2.26$ is calculated, which is in good agreement with the experimentally observed isotropic value. Even though the magnitude of *D* is highly underestimated in the calculations, which indicates a slightly different geometric structure **2**, the theoretical calculations provide a qualitative insight in the electronic structure of **2** and are in line with the experiment.

Further evidence for the bridging motif was gathered by calculating the properties of the monometallic structures (Supporting Information Figures S16 and S17, Tables S4 and S5). In the case of Co(II), a significantly larger ZFS *D*-parameter of $-116.0\ \mathrm{cm}^{-1}$ is calculated for the hypothetical mononuclear species. The anisotropy of the *g*-values is with $g_{\mathrm{x}} = 1.91$, $g_y = 2.02$ and $g_{\mathrm{z}} = 3.29$ also in better agreement with the monomeric heteroleptic complex $[\mathrm{Co(II)bmsab_2}]^{2-}$.[1]

For Ni(II) the *g*-values of the monometallic structure are calculated as $g_{\mathrm{x}} = 2.10$, $g_y = 2.49$ and $g_{\mathrm{z}} = 2.56$ and result in a comparable isotropic g value of $g_{\mathrm{iso}} = 2.38$, which is in the same region as in the dimeric case. In contrast to this, a large, but positive ZFS *D*-parameter of $64.6\ \mathrm{cm}^{-1}$ is found, which is in line with the homoleptic complex that features two bmsab^{2-} ligands[2], but clearly

not with the experimentally observed values and behavior in the case of **2**. For both Co(II) and Ni(II), the dinuclear structures provide a better agreement between calculated and experimentally observed values than the mononuclear models. Hence, DME bridged structures are viable models to reconcile the observed composition of the compounds with their spectroscopic and magnetometric properties in the absence of structural data.

To complete the theoretical picture of the dimer motif, we carried out broken symmetry DFT calculations (PBE0, def2-TZVPP for metal centers and for the first coordination sphere, def2-SVP for all other atoms) on the DFT optimized dimer structures. For **3**, an energy difference of the high-spin state (i.e. both Co(II) spins aligned parallel, leading to a total spin of $S = 3$) and the low-spin state (both spins aligned antiparallel, leading to a singlet state $S = 0$) of $-0.425\ \mathrm{cm}^{-1}$ is found. This energy gap hence suggests an ferromagnetic coupling and transfers to an exchange interaction of $J = -0.1\ \mathrm{cm}^{-1}$ in the $H = J\widehat{\boldsymbol{S}}_1^T\widehat{\boldsymbol{S}}_2$ formalism used in this work.[41-43] The order of magnitude of the exchange interaction in **3** is slightly underestimated compared the experimentally observed exchange, and its sign is calculated opposite. Consequently, the calculated interaction for **3** must be treated with caution. For **2**, the same procedure resulted in a high-spin/low-spin energy gap of $1.353\ \mathrm{cm}^{-1}$ (corresponds to an antiferromagnetic interaction of $J = 0.68\ \mathrm{cm}^{-1}$), which is in good agreement with the experimentally observed exchange interaction of $J_{\mathrm{iso}} = 0.5\ \mathrm{cm}^{-1}$.

FURTHER COMPLEXATION EXPERIMENTS

In order to probe the synthetic applicability of the presented synthons, [M(II)(bmsab)DME] was reacted with 4,4′-di-tert-butyl-2,2′-bipyridyl (DTBBPy) (Scheme 3), leading to the complex **4**.

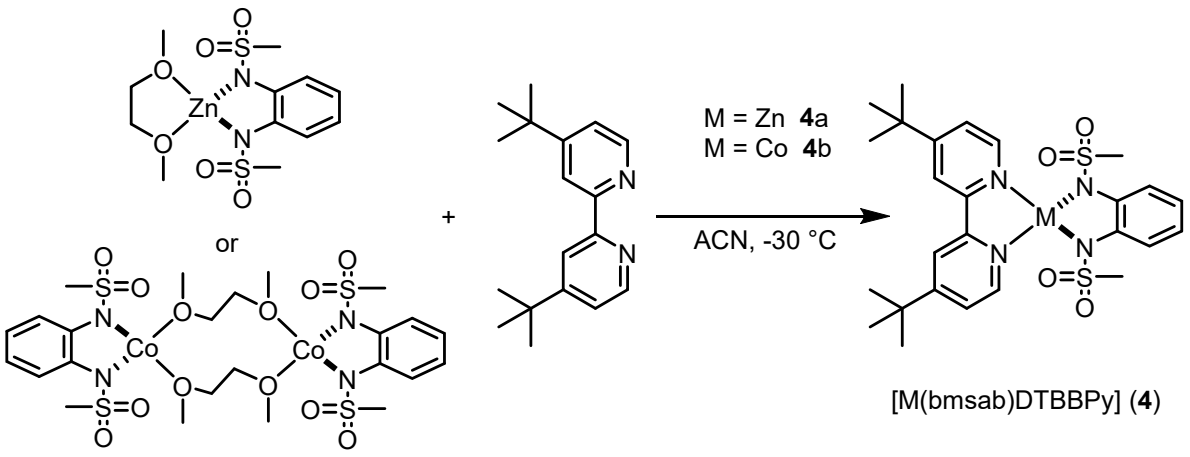

Scheme 3. Complexation experiments carried out with the synthons presented in this work.

The chemical identity of **4**a and **4**b was ensured by means of ^{1}H NMR (for **4**a) and mass spectrometry (MS). For **4**a, three resonances, in line with the DTBBPy ligand, are observed at higher ppm at δ = 8.63 (d, J = 5.54 Hz, 2 H), 8.31 (d, 2 H, J = 1.15 Hz), 7.76 (dd, 2 H, J = 5.63 Hz, 1.76 Hz). The bmsab^{2-} signals are, analogues to **1**, **2** and **3**, observed at 7.39-7.34 (m, 2 H) and 6.88-6.83 (m, 2 H) ppm. Two further singlets are found at 2.89 (s, 6 H) and 1.48 (s, 18 H) ppm. These can be assigned to sulphonamide methyl groups and to the tertbuthyl groups of the DTBBPy ligand (Supporting Information Figure S19).

The complexation experiments highlight the synthetic potential of the presented precursors **1**, **2** and **3**. The range of synthetically accessible complexes via the reaction in scheme 3 could be widened markedly by exchanging DTBBPy to any bidental ligand system. With this, further multinuclear or mononuclear metallic species are thinkable in the context of modern synthetic inorganic chemistry.

CONCLUSIONS

We have presented a series of heteroleptic metal complexes of the stoichiometry [M(II)(bmsab)DME] with M = Co, Ni, Zn. All compounds may serve as versatile precursors for a

variety of molecules with a wide range of desirable properties such as redox activity or single-molecule magnetism. Solution studies show that the DME ligand is only weakly bound and is easily replaced by a coordinating solvent such as acetonitrile. This is a prerequisite for the construction of more complex molecular architectures with this building block. The paramagnetic Ni(II) (**2**) and Co(II) (**3**) complexes behave magnetically different than their homoleptic counterparts. While a large negative ZFS is also present in **3**, no slow relaxation of the magnetization is observed. For **2**, also a large negative ZFS is found. In both cases, intramolecular exchange interactions are experimentally observed and the experimental findings are supported on a theoretical level. This leads to a basic model of the solid state structure of **2** and **3** as $[M(II)(bmsab)DME]_2$ that features a DME bridged dimeric motif. Whereas for the Co(II) complex **3**, a tetrahedral geometry around the metal ion is in line with the experimental findings, for the Ni(II) complex **2**, an octahedral geometry is found. Hence, even without the availability of a crystal structure, a viable structural model for **2** and **3** is established. The magnetic properties are, as in the homoleptic counterparts, dominated by the large ZFS of both paramagnetic systems. In conclusion, this work provides an insight into the chemistry and the physical properties of important synthons of magnetic materials that can be used as building blocks for rational chemical design of new multinuclear materials.

EXPERIMENTAL SECTION

General Remarks and Instrumentation. All syntheses were performed under a dry Ar atmosphere. DME was distilled from K, while hexane and toluene were obtained from a solvent purification system (GS Glovebox Systemtechnik). All solvents were stored over activated molecular sieves and degassed by vigorous bubbling with dry Ar. The ligands H_2bmsab[21] and LiN(Dipp)($SiMe_3$)[22,23] were prepared according to published procedures. Anhydrous $CoCl_2$, anhydrous $ZnCl_2$, NaN($SiMe_3$)$_2$ and LiN($SiMe_3$)$_2$ were obtained from abcr. [$NiCl_2$(DME)] was obtained from Sigma-Aldrich. 4,4'-Di-tert-butyl-bipyridine was obtained from BLDpharm. Commercially available chemicals were used without further purification.

SQUID Magnetometry. Samples were measured as pressed powder pellets wrapped in teflon tape. The instrument used was a Quantum Design MPMS3 SQUID magnetometer. Data were corrected for ferromagnetic impurities as well as for the diamagnetic contribution to the susceptibility by means of Pascal's constants.[24]

High-field EPR. HFEPR measurements were carried out in a frequency range from 230 GHz to 375 GHz at a temperature of 5 K on a homebuilt spectrometer.[25] In this setup, an amplifier-multiplier chain (VDI) is used to obtain the desired frequency. The initial radiation is generated by a synthesizer at a frequency of up to 20 GHz. The radiation is propagated via a quasi-optical setup (Thomas Keating) to the sample and then to the detector (QMC InSb hot electron bolometer). The sample is placed in an Oxford Instruments 15/17T cryomagnet, equipped with a VTI which is allowing temperatures from 1.5K to 300K. The HFEPR data was collected on the same pellets as the SQUID magnetometry data.

EPR. EPR spectra at X-band frequencies were measured on a Bruker EMX spectrometer, equipped with an Oxford 4102ST flow cryostat and a standard TE102 cavity. Measurements were carried out in quartz glass tubes.

Simulations. All simulations were carried out with the EasySpin toolbox (Version 5.2.35) for Matlab (R2021b).[26]

Quantum chemical calculations. All quantum chemical calculations were carried out with the ORCA quantum chemistry program package (Version 5.0.3).[31] Geometry optimizations were performed on DFT level using the PBE0 functional. The Spin Hamiltonian parameters were calculated on CASSCF level. For the metal centres and the first coordination sphere, the def2-TZVPP basis set was used. For the other atoms, the def2-SVP basis set was used. Self-consistent field calculations were tightly converged by using the "tightscf" keyword. For sample inputs, see the supporting information.

Synthesis of the divalent metal amides

Bis(bis(trimethylsilyl)amido)cobalt(II) - THF adduct

The synthetic procedure was adapted from the literature.[27] $Na(N(SiMe_3)_2)$ (3.67 g, 20 mmol, 2 eq.) is dissolved in THF. Anhydrous $CoCl_2$ (1.3 g, 10 mmol, 1 eq.) is suspended in THF and cooled to 0 °C. The $Na(N(SiMe_3)_2)$ solution is added dropwise via canula to the $CoCl_2$ slurry under vigorous stirring. The reaction mixture is stirred and allowed to warm to room temperature overnight, resulting in a dark green solution and copious precipitate. After removal of volatiles, the product is extracted with 60 ml of hexane and filtered over a Celite-padded Schlenk frit. After removal of volatiles, the crude green product is purified by sublimation ($1 \cdot 10^{-3}$ mbar, 75 °C) to yield the pure product as a bright green solid (2.08 g, 46 %). The analytical data agree with the literature.

^{1}H NMR (250 MHz, 25 °C, C_6D_6) δ = 170.85 (4 H, THF), 101.99 (4 H, THF), –17.45 (36 H, SiMe3) ppm.

Bis(bis(trimethylsilyl)amido)zinc(II)

The synthetic procedure was adapted from the literature.[28] $Na(N(SiMe_3)_2)$ (3.67 g, 20 mmol, 2 eq.) and anhydrous $ZnCl_2$ (1.56 g, 10 mmol, 1 eq.) are suspended in 60 ml diethyl ether and stirred under reflux conditions for 4 h. After cooling down and removal of volatiles, the product is extracted with 60 ml of hexane and filtered over a Celite-padded Schlenk frit. After removal of volatiles, the crude product is purified by distillation ($1 \cdot 10^{-3}$ mbar, 85 °C) to yield the pure product as a colorless oil (1.86 g, 48 %). The analytical data agree with the literature. ^{1}H NMR (250 MHz, 25 °C, C_6D_6) δ = 0.2 ppm.

Bis(N-diisopropylphenyl-N-trimethylsilylamido)nickel(II)

The synthetic procedure was adapted from the literature.[15] A 250 ml Schlenk flask was charged with $Li(N(Dipp)(SiMe_3))$ (5 g, 19.57 mmol, 2 eq.) and $NiCl_2$(DME) (2.15 g, 9.78 mmol, 1 eq.). Toluene (80 ml) was added and the reaction mixture was stirred for 12 h, resulting in an intensely colored purple solution and copious precipitate. After removal of volatiles, the solid was extracted with hexane (60 ml) and filtered over a Celite-padded Schlenk frit. The solution was concentrated under high vacuum until crystallization commenced and subsequently stored at –80 °C for 20 h which gave deep purple crystals. The crystalline material was isolated by filtration and dried under high vacuum to give the pure product (0.8 g, 15 % yield). The analytical data agree with the literature.

^{1}H NMR (250 MHz, 25 °C, C_6D_6): δ = 66.75 (4 H), 57.05 (4 H), 42.16 (12 H), 12.00 (12 H), 6.53 (18 H), –93.33 (2 H) ppm.

Synthesis of heteroleptic precursors [M^{II}(bmsab)DME] (M = Co, Ni, Zn)

General procedure: A Schlenk flask is charged with finely powdered H_2bmsab (0.26 g, 1 mmol, 1 eq.), to which dimethoxyethane is added (10 ml). The suspension is cooled to –20 °C. The diamido metal complex (1.1 mmol, 1.1 eq.) is dissolved in dimethoxyethane (Co, Zn) or toluene (Ni) and the solution is added dropwise to the slurry of H_2bmsab. The reaction mixture is brought to room temperature over the course of 1.5 h and then stirred for an additional 1.5 h, after which approximately half of the solvent is removed. Hexane (10 ml) is added and the reaction mixture stirred for 10 min. The supernatant is filtered off and the product is obtained as a fine powder after drying under high vacuum for 6 h. The products are air- and moisture-sensitive and hardly soluble in their native form. At this point, CHNS analysis appears to be the only feasible way of determining the purity of the product.

[Co(bmsab)DME] Obtained as a pink powder in 65 % yield.

Anal. calcd. for $C_{12}H_{20}N_2CoO_6S_2$: C 35.04, H 4.90, N 6.81, S 15.59; found: C 35.13, H 5.07, N 6.67, S 15.08.

[Ni(bmsab)DME] Obtained as a maroon powder in 42 % yield.

Anal. calcd. for $C_{12}H_{20}N_2NiO_6S_2$: C 35.06, H 4.90, N 6.81, S 15.60; found: C 35.09, H 5.098, N 6.60, S 14.89.

[Zn(bmsab)DME] Obtained as a colorless powder in 73 % yield.

Anal. calcd. for $C_{12}H_{20}N_2ZnO_6S_2$: C 34.50, H 4.83, N 6.71, S 15.35; found: C 33.89, H 4.93, N 6.50, S 15.07.

Synthesis of [M(bmsab)DTBBPy] (M = Zn, Co)

General Procedure: A Schlenk flask was charged with the respective heteroleptic precursor (40 mg, 1 eq.), cooled to -20 °C and acetonitrile (10 ml) was added. 4,4′-di-tert-butyl-2,2′-bipyridyl (1 eq.) was dissolved in acetonitrile (5 ml) and added dropwise to the solution of the heteroleptic precursor at -20 °C. The mixture was stirred for 2 h, the solvent was removed and the resulting powder dried under high vacuum.

[Zn(bmsab)DTBBPy] Obtained as off-white powder in 85 % yield.

^{1}H NMR (400 MHz, 25 °C, CD_2Cl_2): 8.63 (d, J = 5.54 Hz, 2 H), 8.32 (s, 2 H), 7.72 (bs, 2 H), 7.36 (m, 2 H), 6.85 (m, 2 H), 2.89 (s, 6 H), 1.47 (s, 18 H) ppm

(+)-ESI: $\frac{m}{z}$: 595.14 $[M]^+$, *Signal matches with the simulated signal for* $C_{26}H_{34}N_4O_4S_2Zn$ 617.12 $[M+Na]^+$, 269.20 $[dtbbpy]^+$

[Co(bmsab)DTBBPy] Obtained as dark red powder in 82 % yield.

(+)-ESI: $\frac{m}{z}$: 589.13 $[M]^+$, 269.20 $[dtbbpy+H]^+$, 287.01 $[bmsab+Na]^+$

ASSOCIATED CONTENT

Supporting Information

The following files are available free of charge:

Additional experimental data (PDF)

AUTHOR INFORMATION

Corresponding Authors

Biprajit Sarkar, Lehrstuhl für Anorganische Koordinationschemie, Institut für Anorganische Chemie, Universität Stuttgart, Pfaffenwaldring 55, 70569 Stuttgart, Germany

*biprajit.sarkar@iac.uni-stuttgart.de

Joris van Slageren, Institut für Physikalische Chemie, Universität Stuttgart, Pfaffenwaldring 55, 70569 Stuttgart, Germany

*slageren@ipc.uni-stuttgart.de

Author Contributions

B.S. and J.v.S. conceived the research and supervised the work. Synthetic work, NMR- and UV/Vis/NIR spectroscopy was performed by S. S. Magnetic characterization and EPR spectroscopy was performed and analyzed by D. H. The complexation tests were carried out by V. B. The manuscript was written through contributions of all authors. All authors have given approval to the final version of the manuscript. ‡These authors contributed equally.

Funding Sources

This work was funded by the Landesgraduiertenförderung Baden-Württemberg, DFG SL104/10-1, SA1840/9-1

Notes

The authors declare no competing interests.

ACKNOWLEDGMENT

We thank Timo Holzmann for the preliminary work on the magnetochemistry and the spectroscopy of the Co(II) complex.

ABBREVIATIONS

bmsab, 1,2-bis(methansulfonamido)benzene; DME, dimethoxyethane; ZFS, zero-field splitting, SQUID, super conducting quantum interference device, HFEPR, High-field electron paramagnetic resonance

REFERENCES

(1) Rechkemmer, Y.; Breitgoff, F. D.; van der Meer, M.; Atanasov, M.; Hakl, M.; Orlita, M.; Neugebauer, P.; Neese, F.; Sarkar, B.; van Slageren, J. A four-coordinate cobalt(II) single-ion magnet with coercivity and a very high energy barrier. *Nat. Commun.* **2016**, *7*, 268.

(2) Bamberger, H.; Albold, U.; Dubnická Midlíková, J.; Su, C.-Y.; Deibel, N.; Hunger, D.; Hallmen, P. P.; Neugebauer, P.; Beerhues, J.; Demeshko, S. *et al.* Iron(II), Cobalt(II), and Nickel(II) Complexes of Bis(sulfonamido)benzenes: Redox Properties, Large Zero-Field Splittings, and Single-Ion Magnets. *Inorg. Chem.* **2021**, *60*, 2953–2963.

(3) Fataftah, M. S.; Zadrozny, J. M.; Rogers, D. M.; Freedman, D. E. A mononuclear transition metal single-molecule magnet in a nuclear spin-free ligand environment. *Inorg. Chem.* **2014**, *53*, 10716–10721.

(4) Cui, H.-H.; Lu, F.; Chen, X.-T.; Zhang, Y.-Q.; Tong, W.; Xue, Z.-L. Zero-Field Slow Magnetic Relaxation and Hysteresis Loop in Four-Coordinate Co(II) Single-Ion Magnets with Strong Easy-Axis Anisotropy. *Inorg. Chem.* **2019**, *58*, 12555–12564.

(5) Albold, U.; Bamberger, H.; Hallmen, P. P.; van Slageren, J.; Sarkar, B. Strong Exchange Couplings Drastically Slow Down Magnetization Relaxation in an Air-Stable Cobalt(II)-Radical Single-Molecule Magnet (SMM). *Angew. Chem. Int. Ed.* **2019**, *58*, 9802–9806.

(6) Jeon, I., Park, J., Xiao, D., Harris, D.; An Azophenine Radical-Bridged Fe2 Single-Molecule Magnet with Record Magnetic Exchange Coupling. *J. Am. Chem. Soc.* **2013**, *135*, 45, 16845-16848

(7) Rinehart, J., Fang, M., Evans, W., Long, J.; Strong exchange and magnetic blocking in N_2^{3-}-radical-bridged lanthanide complexes. *Nat. Chem.* **2011**, *3*, 538-542

(8) Rinehart, J., Fang, M., Evans, W., Long, J.; A N_2^{3-} Radical-Bridged Terbium Complex Exhibiting Magnetic Hysteresis at 14 K. *J. Am. Chem. Soc.* **2011**, *133*, 36, 14236-14239

(9) Demir, S., Zadrozny, J., Nippe, M., Long, J.; Exchange Coupling and Magnetic Blocking in Bipyrimidyl Radical-Bridged Dilanthanide Complexes. *J. Am. Chem. Soc.* **2012**, *134*, 45, 18546-18549

(10) Pedersen, K. S.; Bendix, J.; Clérac, R. Single-molecule magnet engineering: Building-block approaches. *Chem. Commun.* **2014**, *50*, 4396–4415.

(11) Khusniyarov, M. M.; Weyhermüller, T.; Bill, E.; Wieghardt, K. Reversible electron transfer coupled to spin crossover in an iron coordination salt in the solid state. *Angew. Chem. Int. Ed.* **2008**, *47*, 1228–1231.

(12) Lappert, M. F.; Protchenko, A. V.; Power, P. P.; Seeber, A. L. *Metal Amide Chemistry*, (1. ed.), John Wiley & Sons, Chichester, **2008**.

(13) Faust, M.; Bryan, A. M.; Mansikkamäki, A.; Vasko, P.; Olmstead, M. M.; Tuononen, H. M.; Grandjean, F.; Long, G. J.; Power, P. P. The Instability of $Ni\{N(SiMe_3)_2\}_2$: A Fifty Year Old Transition Metal Silylamide Mystery. *Angew. Chem. Int. Ed.* **2015**, *54*, 12914–12917.

(14) Reckziegel, A.; Battistella, B.; Schmidt, A.; Werncke, C. G. Intricate Road to Linear Anionic Nickel(I) Hexamethyldisilazanide $Ni(N(SiMe_3)_2)_2$. *Inorg. Chem.* **2022**, *61*, 7794–7803.

(15) Lipschutz, M. I.; Tilley, T. D. Synthesis and Reactivity of a Conveniently Prepared Two-coordinate Bis(amido) Nickel(II) Complex. *Chem. Commun.* **2012**, *48*, 7146–7148.

(16) Lever, A. B. P. *Inorganic Electronic Spectroscopy*, (2. ed.), 2. impression (with corr.); Studies in physical and theoretical chemistry 33; Elsevier: Amsterdam, **1986**.

(17) Boča, R. Zero-field Splitting in Metal Complexes. *Coord. Chem. Rev.* **2004**, *248*, 757–815.

(18) Jiang, S.-D.; Maganas, D.; Levesanos, N.; Ferentinos, E.; Haas, S.; Thirunavukkuarasu, K.; Krzystek, J.; Dressel, M.; Bogani, L.; Neese, F. *et al.* Direct Observation of Very Large Zero-Field Splitting in a Tetrahedral Ni(II)Se_4 Coordination Complex. *J. Am. Chem. Soc.* **2015**, *137*, 12923–12928.

(19) van Slageren, J.; Vongtragool, S.; Gorshunov, B.; Mukhin, A. A.; Karl, N.; Krzystek, J.; Telser, J.; Müller, A.; Sangregorio, C.; Gatteschi, D. *et al.* Frequency-domain Magnetic Resonance Spectroscopy of Molecular Magnetic Materials. *Phys. Chem. Chem. Phys.* **2003**, *5*, 3837–3843.

(20) Kowal, A. T.; Zambrano, I. C.; Moura, I.; Moura, J. J. G.; LeGall, J.; Johnson, M. K. Electronic and Magnetic Properties of Nickel-substituted Rubredoxin: A Variable-temperature Magnetic Circular Dichroism Study. *Inorg. Chem.* **1988**, *27*, 1162–1166.

(21) Cheng, H.-Y.; Cheng, P.-H.; Lee, C.-F.; Peng, S.-M. A Versatile Ligand for Coordination Chemistry: Metal Complexes of Alkyl- or Arylsulfonyl Amides. *Inorg. Chim. Acta* **1991**, *181*, 145–147.

(22) Chao, Y. W.; Wexler, P. A.; Wigley, D. E. Preparation and Properties of Tantalum Imido Complexes and their Reactions with Alkynes. Coordination Control through Multiple Metal-ligand Bonding. *Inorg. Chem.* **1989**, *28*, 3860–3868.

(23) Kennepohl, D. K.; Brooker, S.; Sheldrick, G. M.; Roesky, H. W. Synthesis and Molecular Structure of the Solvent-Free [$LiN(SiMe_3)(2,6\text{-}^iPr_2C_6H_3)]_2$ Dimer. *Chem. Ber.* **1991**, *124*, 2223–2225.

(24) Bain, G. A.; Berry, J. F. Diamagnetic Corrections and Pascal's Constants. *J. Chem. Educ.* **2008**, *85*, 532.

(25) Neugebauer, P.; Bloos, D.; Marx, R.; Lutz, P.; Kern, M.; Aguilà, D.; Vaverka, J.; Laguta, O.; Dietrich, C.; Clérac, R. *et al.* Ultra-broadband EPR Spectroscopy in Field and Frequency Domains. *Phys. Chem. Chem. Phys.* **2018**, *20*, 15528–15534.

(26) Stoll, S.; Schweiger, A. EasySpin, a Comprehensive Software Package for Spectral Simulation and Analysis in EPR. *J. Magn. Reson.* **2006**, *178*, 42–55.

(27) Power, P. P. (Ed.) *Inorganic Syntheses: Volume 37;* John Wiley and Sons, Hoboken, **2018**.

(28) Yang, R.; Xu, G.; Lv, C.; Dong, B.; Zhou, L.; Wang, Q. $Zn(HMDS)_2$ as a Versatile Transesterification Catalyst for Polyesters Synthesis and Degradation toward a Circular Materials Economy Approach. *ACS Sustainable Chem. Eng.* **2020**, *8*, 18347–18353.

(29) Shao, D.; Moorthy, S.; Zhou, Y.; Wu, S.; Zhu, J.; Yang, J.; Wu, D.; Tian, Z.; Singh, S. K.; Field-induced slow magnetic relaxation behaviours in binuclear cobalt(II) metallocycles and exchange-coupled clusters. *Dalton Trans.* **2022**, *51*, 9357

(30) Ferreira, P., Cerdeira, A., Cruz, T., Bandeira, N., Hunger, D., Allgaier, A., van Slageren, J., Almeida, M., Pereira, L., Gomes, P.; Single-ion magnet behavior in homoleptic Co(II) complexes bearing 2- iminopyrrolyl ligands. *Inorg. Chem. Front.* **2022**, 9, 4302

(31) Neese, F, Wennmohs, F. Becker, U., Riplinger C.; The ORCA quantum chemistry program package. *J. Chem. Phys.* **2020**, 152, 224108

(32) Gransbury, G., Boulon, M., Mole, R., Gable, R., Moubaraki, B., Murray, K., Sorace, L., Soncini, A., Boskovic, C.; Single-ion anisotropy and exchange coupling in cobalt(II)-radical complexes: insights from magnetic and ab initio studies. *Chem. Sci.* **2019**, 10, 8855

(33) Misochko, E., Akimov, A., Korchagin, D., Nehrkorn, J., Ozerov, M., Palii, A., Clemente-Juan, J., Aldoshin, S.; Purely Spectroscopic Determination of the Spin Hamiltonian Parameters in High-Spin Six-Coordinated Cobalt(II) Complexes with Large Zero-Field Splitting. *Inorg. Chem.* **2019**, 58, 16434

(34) Ruiz, E., Cano, J., Alvarez, S., Alemany, P.; Broken Symmetry Approach to Calculation of Exchange Coupling Constants for Homobinuclear and Heterobinuclear Transition Metal Complexes. *J. Comput. Chem.* **1999**, 20, 1391-1400

(35) Atanasov, M., Comba, P., Helmle, S., Müller, D., Neese, F.; Zero-Field Splitting in a Series of Structurally Related Mononuclear Ni(II)−Bispidine Complexes. *Inorg. Chem.* **2012**, 51, 12324-12335

(36) Titis, J., Boca, R.; Magnetostructural *D* Correlation in Nickel(II) Complexes: Reinvestigation of the Zero-Field Splitting. *Inorg. Chem.* **2010**, 49, 3971-3973

(37) Herchel, R., Boca, R., Krzystek, J., Ozarowski, A., Duran, M., van Slageren, J.; Definitive Determination of Zero-Field Splitting and Exchange Interactions in a Ni(II) Dimer: Investigation of $[Ni_2(en)_4Cl_2]Cl_2$ Using Magnetization and Tunable-Frequency High-Field Electron Paramagnetic Resonance. *J. Am. Chem. Soc.* **2007**, 2007, 129, 10306-10307

(38) Desrochers, P. J., Telser, J., Zvyagin, S.A., Ozarowski, A., Krzystek J., Vicic, D. A.; Electronic Structure of Four-Coordinate C_{3v} Nickel(II) Scorpionate Complexes: Investigation by

High-Frequency and -Field Electron Paramagnetic Resonance and Electronic Absorption Spectroscopies. *Inorg. Chem.* **2006**, 45, 8930-8941

(39) Maslejova, A., Boca, R., Dlhan, L., Papankova, B., Svoboda, I., Fuess, H.; Structure and zero-field splitting in bis(1,2-dimethylimidazole)bis(acetato)nickel(II) molecular complex. *Chem. Phys. Lett.* **2001**, 347, 397-402

(40) Boca, R., Dlhan, L., Haase, W., Herchel, R., Maslejova, A., Papankova, B.; Limiting negative zero-field splitting in tetrakis(imidazole)bis(acetato) nickel(II) complex. *Chem. Phys. Lett.* **2002**, 373, 402-410

(41) Ginsberg, A.P.; Magnetic exchange in transition metal complexes. 12. Calculation of cluster exchange coupling constants with the X-alpha-scattered wave method. *J. Am. Chem. Soc.* **1980**, 102, 1, 111-117

(42) Noodleman, L.; Valence bond description of antiferromagnetic coupling in transition metal dimers. *J. Chem. Phys.* **1981**, 74, 5737-5743

(43) Noodleman, L., Davidson, E. R.; Ligand spin polarization and antiferromagnetic coupling in transition metal dimers. *Chem. Phys.*, **1986**, 109, 1, 131-143

(44) Ogoshi, S., Ikeda, H., Kurosawa, H.; *Angew. Chem. Int. Ed.,* **2007**, 46, 4930

(45) Davies, J., Janssen-Müller, D., Zimin, D. P., Day, C. S., Yanagi, T., Elfert, J., Martin, R.; *J. Am. Chem. Soc.* **2021**, 143, 4949

(46) Sousa-Pedrares, A., Viqueira J. A., Antelo, J., Labisbal, E., Romero, J., Sousa, A., Nascimento, O. R., García-Vázquez, J. A.; *Eur. J. Inorg. Chem.* **2011**, 2011, 2273

FOR TABLE OF CONTENTS ONLY

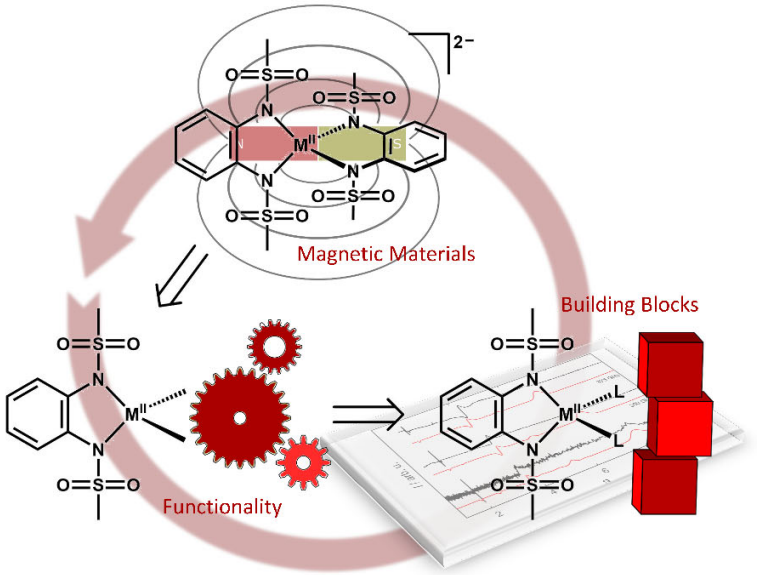

The synthesis and a thorough magnetic, spectroscopic and theoretical investigation is presented on useful precursor molecules that are valuable synthons for the tailored bottom-up synthesis of magnetic materials.

Precursor molecules for cobalt(II) single molecule magnets – Synthesis and magnetic properties

David Hunger[‖,‡], *Simon Suhr*[⊥,‡], *Valentin Bayer*[‖], *Uta Albold*[§], *Biprajit Sarkar*[⊥,*], *Joris van Slageren*[‖,*]

[‖] Institut für Physikalische Chemie, Universität Stuttgart, Pfaffenwaldring 55, 70569 Stuttgart, Germany

[⊥] Institut für Anorganische Chemie, Universität Stuttgart, Pfaffenwaldring 55, 70569 Stuttgart, Germany

[§] Institut für Anorganische Chemie, Freie Universität Berlin, Fabeckstraße 34-36, 14195 Berlin, Germany

[‡] Equal Contribution

Contents

NMR Spectra

[Zn(II)(bmsab)dme]

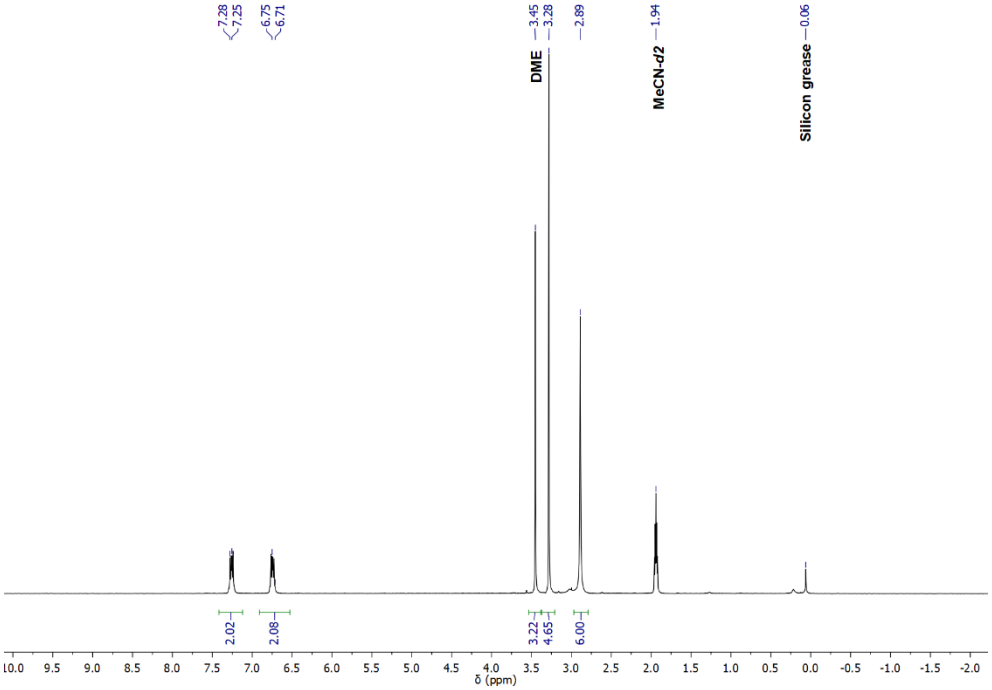

Figure S1: ^{1}H-NMR-Spectrum (250 MHz, MeCN-*d3*, 25 °C) of the heteroleptic Zn(II) precursor **[Zn^{II}(bmsab)dme]** dissolved in deutero-acetonitrile.

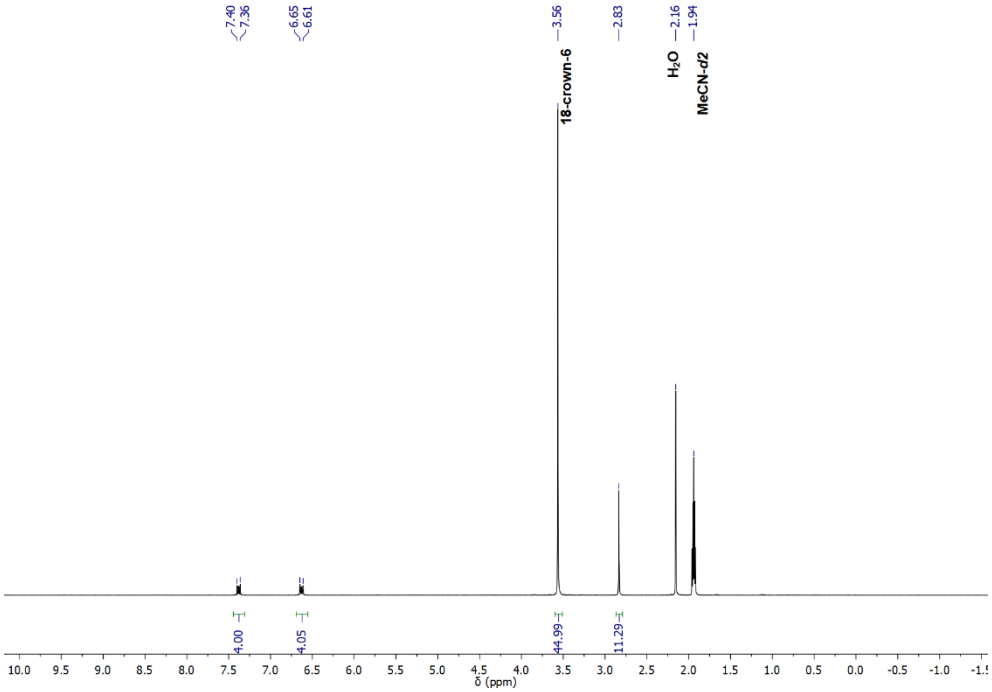

Figure S2: ^{1}H-NMR-Spectrum (250 MHz, MeCN-*d3*, 25 °C) of the homoleptic complex **(K-18-crown-6)$_2$[Zn^{II}(bmsab)$_2$]** dissolved in deutero-acetonitrile.

[Ni(II)(bmsab)dme]

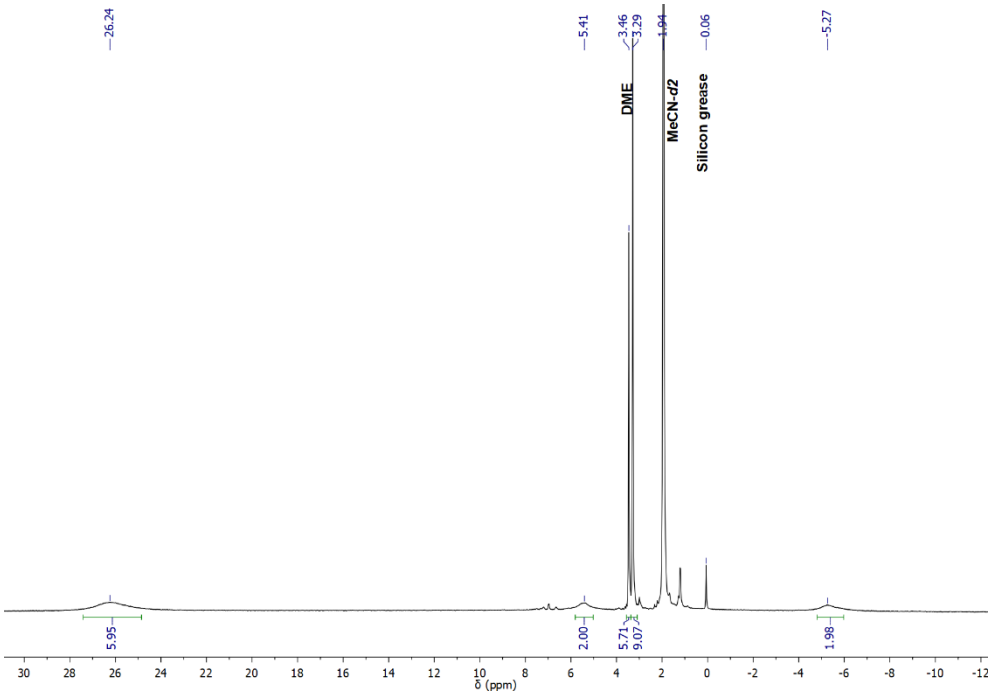

Figure S3: ^{1}H-NMR-Spectra (250 MHz, MeCN-*d3*, 25 °C) of the heteroleptic Ni(II) precursor **[Ni^{II}(bmsab)dme]** dissolved in deutero-acetonitrile.

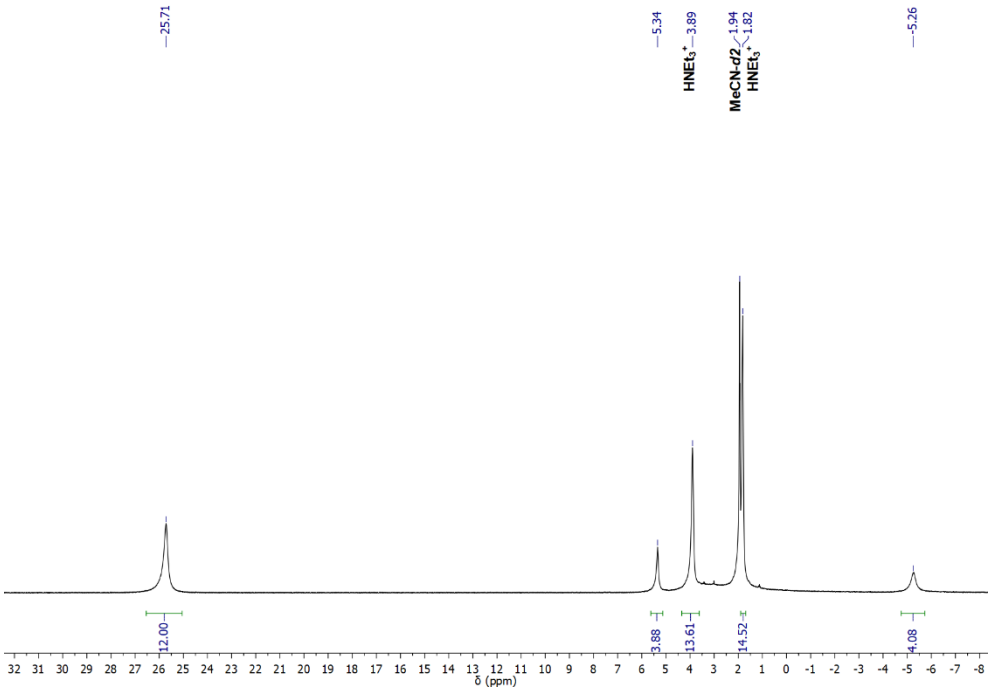

Figure S4: ^{1}H-NMR-Spectrum (250 MHz, MeCN-*d3*, 25 °C) of the homoleptic Ni(II) complex **(HNEt$_3$)$_2$[Ni^{II}(bmsab)$_2$]** dissolved in deutero-acetonitrile.

[Co(II)(bmsab)dme]

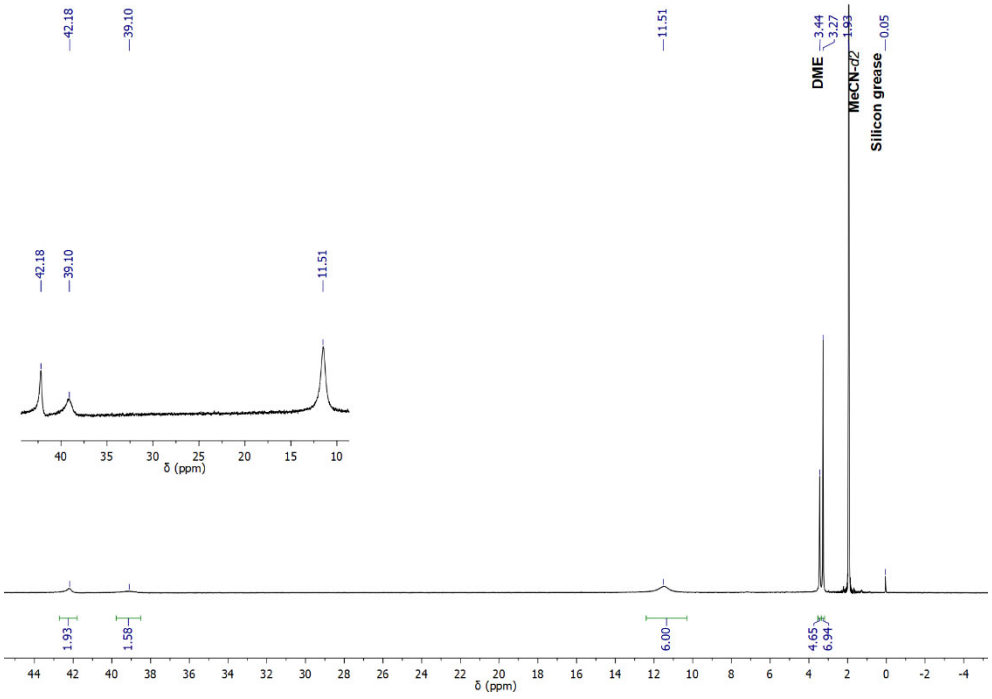

Figure S5: ^{1}H-NMR-Spectrum (250 MHz, MeCN-*d3*, 25 °C) of the heteroleptic Co(II) precursor **[Co^{II}(bmsab)dme]** dissolved in deutero-acetonitrile.

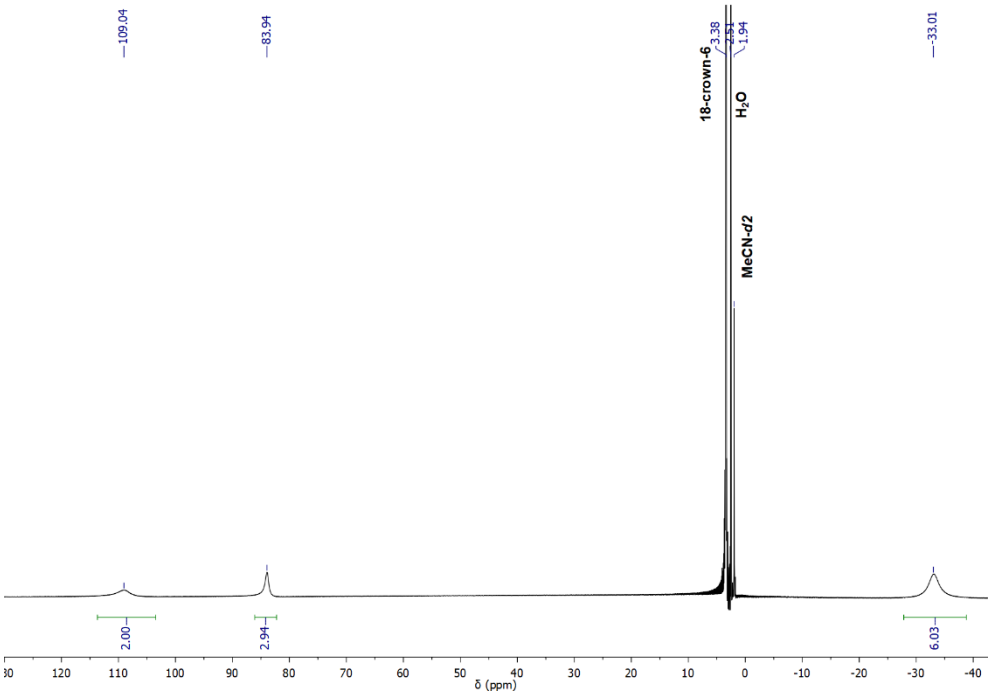

Figure S6: ^{1}H-NMR-Spectrum (250 MHz, MeCN-*d3*, 25 °C) of the homoleptic Co(II) complex **(K-18-crown-6)$_2$[Co^{II}(bmsab)$_2$]** dissolved in deutero-acetonitrile.

UV/Vis/NIR Spectroscopy

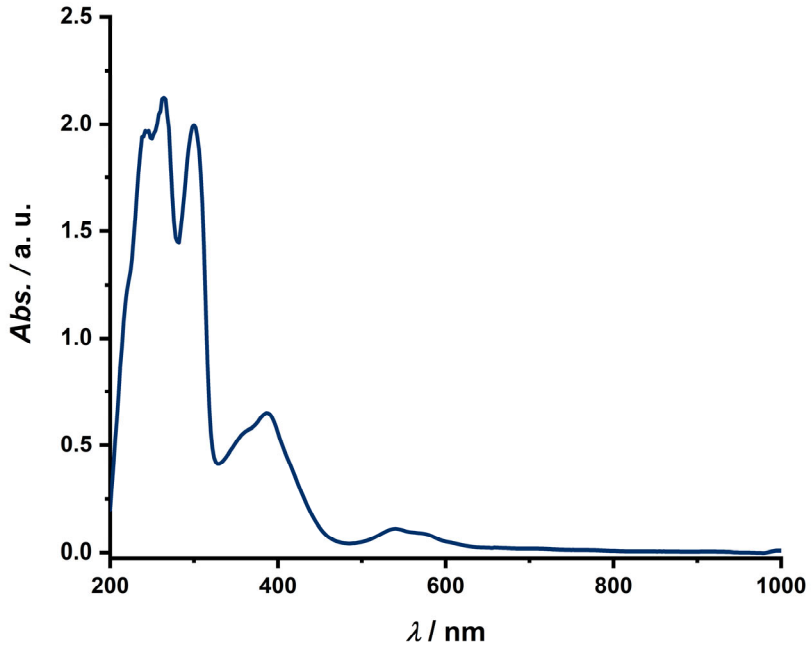

Figure S7: UV/Vis/NIR spectrum of heteroleptic precursor **[Ni^{II}(bmsab)dme] (2)** dissolved in acetonitrile**.**

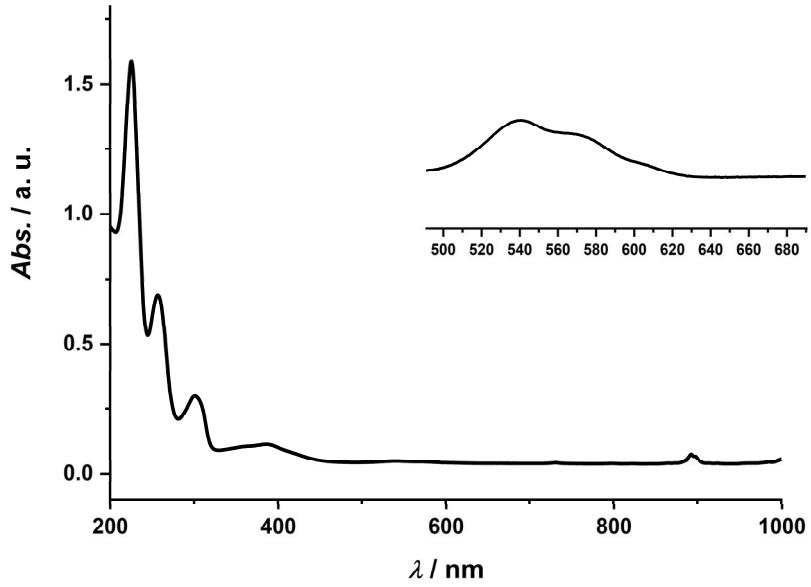

Figure S8: UV/Vis/NIR spectrum of the homoleptic complex **[Ni^{II}(bmsab)$_2$]$^{2-}$** dissolved in acetonitrile. Inset shows the bands between 540 and 570 nm at higher concentration. Compound was re-measured as the weak low-wavelength bands were not mentioned in the original publication[1].

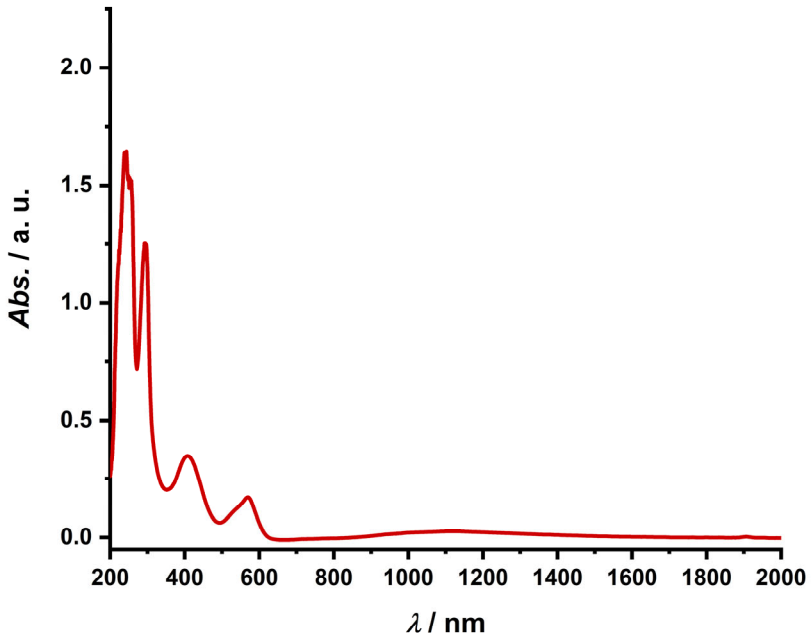

Figure S9: UV/Vis/NIR spectrum of heteroleptic precursor **[Co^{II}(bmsab)dme] (3)** dissolved in acetonitrile.

Table S1: Absorption maxima of acetonitrile solutions of the heteroleptic precursors **2** and **3** and of the corresponding homoleptic complexes. Values for **[Co^{II}(bmsab)$_2$]$^{2-}$** were taken from reference 1.

	Absorption maxima / nm
[Ni^{II}(bmsab)dme] (2)	244, 264, 300, 386, 540, 574
[Ni^{II}(bmsab)$_2$]$^{2-}$	230, 256, 301, 389, 540, 568
[Co^{II}(bmsab)dme] (3)	244 257, 295, 408, 569, 1120
[Co^{II}(bmsab)$_2$]$^{2-}$	234, 259, 305, 561

SQUID Magnetometry

For all measurements potential ferromagnetic impurities were corrected for. To this end, temperature dependent susceptibility measurements were carried out in the temperature regime from 1.8 K up to 50 K at an applied magnetic field of 1000 Oe and from 40 K to 300 K at an applied field at 10000 Oe. The overlap region served for correcting the data for the ferromagnetic impurity. The diamagnetic contribution was estimated on the basis of Pascal's constants.[3]

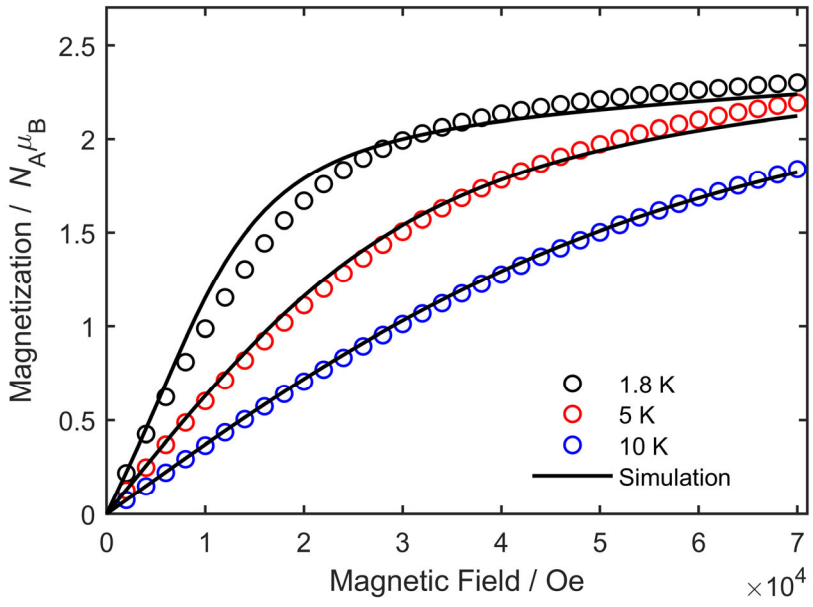

Figure S10: Magnetization curves of the heteroleptic precursor **[Co^{II}(bmsab)dme] (3)** at the indicated temperatures. Experimental values are shown as circles, while spin Hamiltonian simulations at the corresponding temperatures are shown as black lines. Simulations are carried out with the parameters given in the main text.

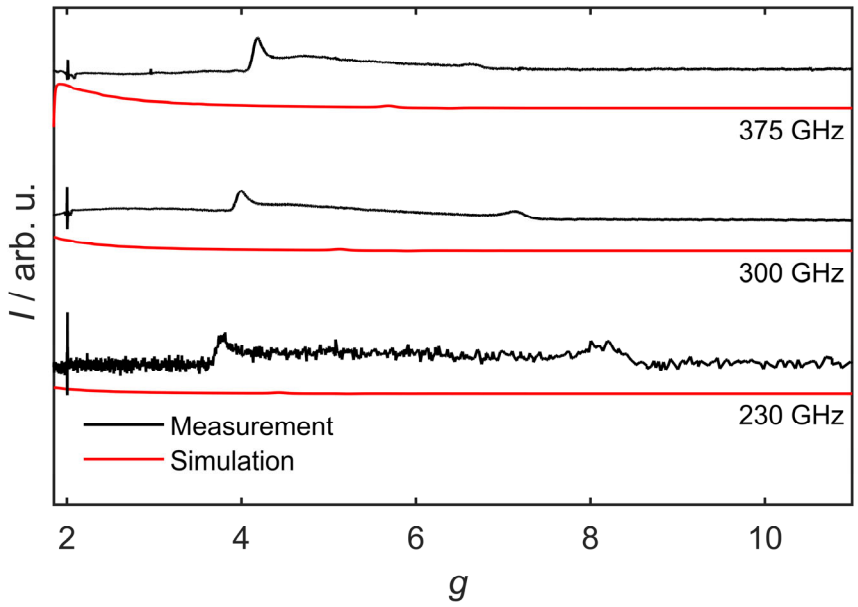

Figure S11: Measured HFEPR spectra of **3** at the indicated frequencies at 5 K (black), simulations based on the parameter set, that was obtained on the basis of the magnetometry measurements are shown in red.

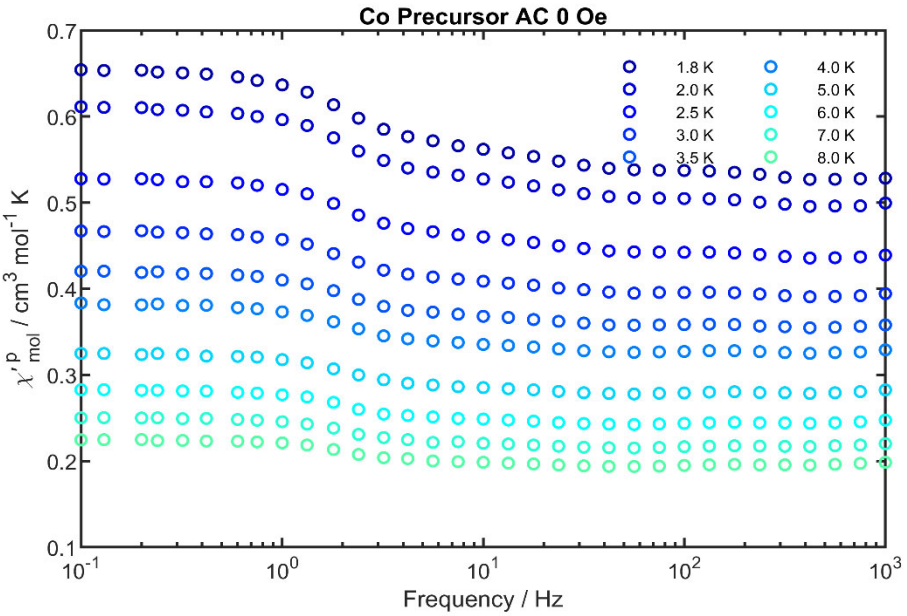

Figure S12: In-phase component of the dynamic susceptibility of the heteroleptic precursor **[Co^{II}(bmsab)dme] (3)** at the indicated temperatures in zero applied magnetic field.

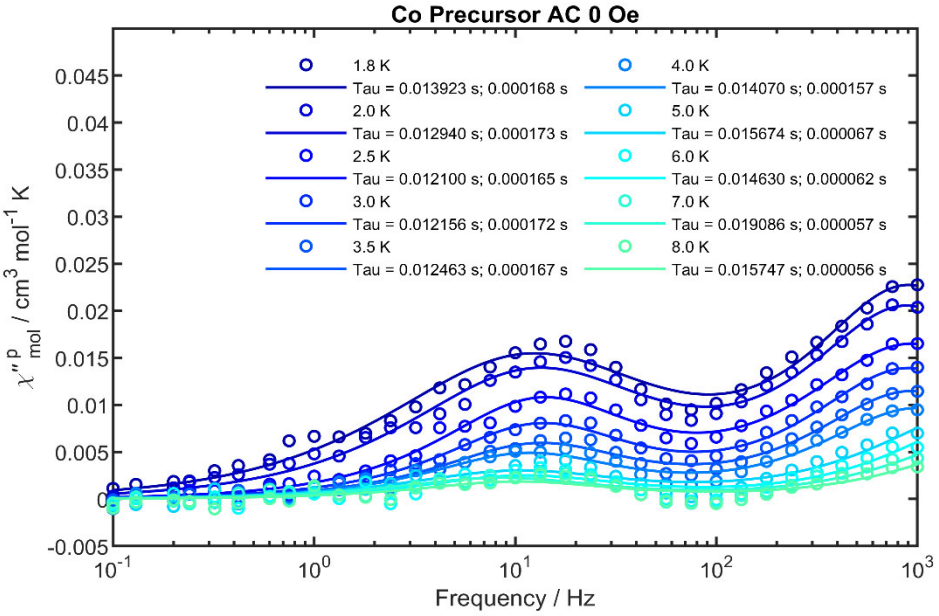

Figure S13: Out-of-phase component of the dynamic susceptibility of the heteroleptic precursor **[Co^{II}(bmsab)dme] (3)** at the indicated temperatures in zero applied magnetic field. The solid lines are fits based on modified Debye functions. Two relaxation processes with different relaxation times are visible and hence two relaxation times are given at each temperature. Since the magnitude of $X``$ is only approx. 3% of $X`$, the out-of-phase signal is attributed to an impurity.

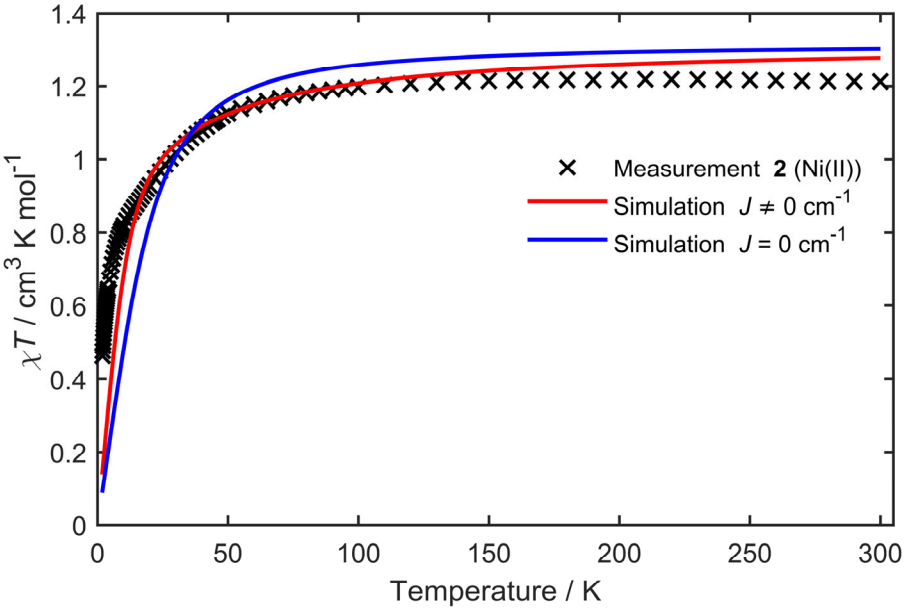

Figure S14: Temperature-susceptibility curve of **2** (black symbols) and the corresponding simulations based on the assumption of a **positive** *D* parameter. The parameters are given in table 1 in the main text.

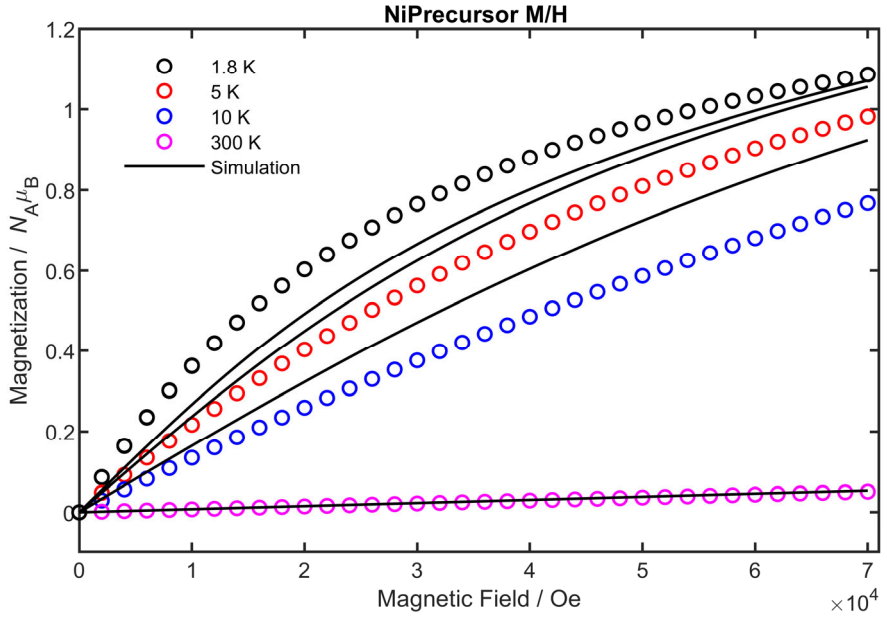

Figure S15: Magnetization curves of the heteroleptic precursor **[Ni^{II}(bmsab)dme] (2)** plotted as magnetic moment versus field at the temperatures indicated. Measurements are shown as circles, while the simulations are shown as black solid lines. The simulations are based on the parameters given in table 1 in the main text, that feature a **positive** ZFS *D* parameter.

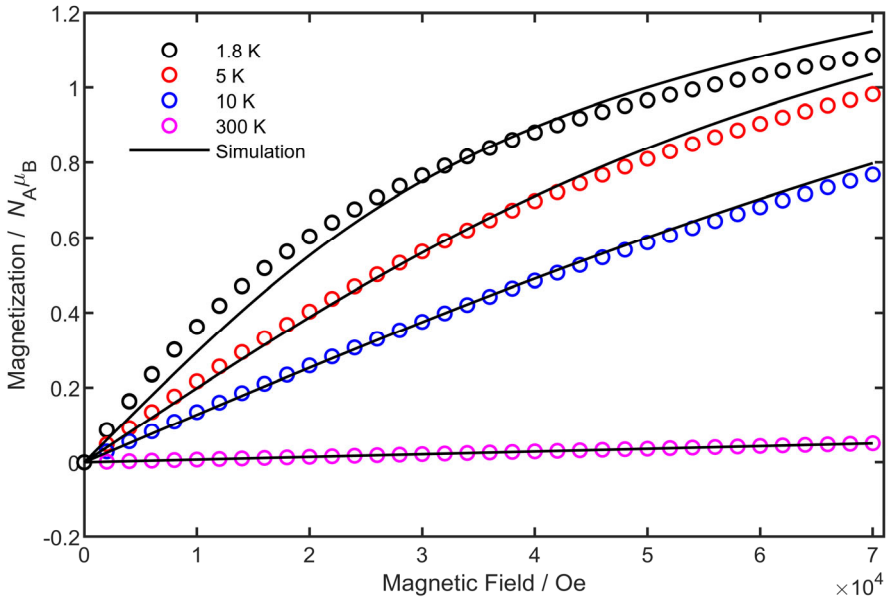

Figure S16: Magnetization curves of **[Ni^{II}(bmsab)dme] (2)**, measured at the indicated temperatures (circles). The corresponding simulations are based on eq. (1) and are carried out under the assumption of a **negative** ZFS *D* parameter (see table 1 in the main text).

Theoretical Calculations

Table S2: Geometry optimized coordinates of the dimer of [Co^{II}(bmsab)dme] (**3**)

C	-2.17194417265913	1.38773331712138	-0.66167156160106
C	-2.02569144086611	0.26227930860450	-1.46743940300876
C	-0.80546664054372	-0.41467862063060	-1.51814083365710
C	0.26922016617229	0.01462865790177	-0.73575717723295
C	0.11950904377610	1.16930825988355	0.08330969167759
C	-1.09907142639480	1.85027550723508	0.10198935452665
N	1.27665988739635	1.50659334429055	0.78780135455300
N	1.54510846294699	-0.56145843551830	-0.67636113283559
S	1.52819686832365	2.82179374685961	1.68596952874434
S	1.99405953850836	-1.91327066057873	-1.42811114871310
O	3.42049638976900	-2.06399580448456	-1.03873534603296
O	1.68156807927113	-1.94946458121166	-2.85562270884415
O	2.98756815701559	2.75775555298036	1.95240647082242
O	0.98090087378496	4.05241363824771	1.12326916974625
C	0.72310626242939	2.56491356126601	3.25628332207351
H	1.14664806641852	1.67324386382787	3.73263717720399
H	-0.35510802735168	2.44945744078962	3.08574018077729
H	0.91983201133665	3.46267886173947	3.85672238374351
C	1.11570310230877	-3.27256383505711	-0.67513616279642
H	1.42588509058300	-4.17727040661226	-1.21357847200737
H	0.03747032595934	-3.10686639157592	-0.79588123080473
H	1.38591347464604	-3.33420228413205	0.38524532086950
Co	2.87210839048619	0.51063486075688	0.30602132592870

Co	8.10494763941323	0.44664209144323	-0.02758298367423
N	9.53485514426795	1.64759928904898	-0.64631655181494
N	9.62862711402653	-0.70324253118249	0.35285723527638
C	10.88359636657700	-0.15953039860739	0.06991359697640
C	10.83476671026517	1.16425352726627	-0.44913157349414
C	12.02957876210667	1.84309357503096	-0.70129811762825
C	12.11747195904398	-0.79028922590319	0.24654454209305
C	13.30019302680738	-0.10525036273773	-0.03710608772865
C	13.25601555883683	1.20746009126320	-0.49761926703988
S	9.34918624990524	-2.00157594399785	1.26899607030303
S	9.16322816048632	3.12441912740337	-1.17482087798023
O	9.85799309493200	4.20048181783893	-0.46946578240176
O	7.67929338629405	3.13432772722569	-1.15869388521643
O	10.05401568797966	-3.20925669111458	0.84828600179937
O	7.86729939486348	-2.04404522748735	1.33361207689649
C	9.64428619618119	3.23297908543561	-2.89076393144071
H	10.72754987730580	3.07743238036375	-2.96974040558823
H	9.37801417162808	4.24495580336781	-3.22242387950170
H	9.09921736273626	2.47396171906110	-3.46428197977608
C	9.92172116229228	-1.62212334831236	2.91783712307161
H	10.99948492404168	-1.41738093723920	2.87858396541010
H	9.72480025149097	-2.51419599977512	3.52638896488608
H	9.36962958469633	-0.75395476218679	3.29676453146503
H	14.18121500562967	1.75202856663391	-0.69980956966359
H	14.25983266487323	-0.60759738527450	0.10495509947863
H	12.14042311228269	-1.82795436622615	0.58607672578481
H	12.00157531987217	2.88658127220759	-1.02002074635411
H	-1.19244141353321	2.76823701299268	0.68495987752328
H	-3.11980512053288	1.93036208577091	-0.63962274787623
H	-2.85722967459856	-0.08477643829525	-2.08505228371346
H	-0.67154675266653	-1.25589059132461	-2.20084536583545
O	3.94381240322947	-0.44002736961659	1.81718385617624
O	4.27738337171699	1.38570228424658	-0.94443161513391
O	6.74429867744392	-0.24329968289577	-1.40573533696585
O	7.11160448815042	1.28771535394828	1.61056984396902
C	4.63150138234371	0.73298085900108	-2.17027658952806
C	6.12562383548379	0.62417669825032	-2.36067585807435
H	4.19781649861794	1.29417303282394	-3.01561870091068
H	4.15986562081246	-0.25827639360772	-2.14181527890436
H	6.61925511540135	1.60068935726547	-2.24610170816365
H	6.32876280662816	0.24167736292904	-3.37598575779728
C	5.37262466678175	-0.37951175994488	1.73394945752986
C	5.78658213449800	1.03678281802498	2.07421654613076
H	5.69274476880404	-0.65996661310129	0.71962862945773
H	5.81460828533048	-1.11265087718414	2.42188673157321
H	5.76024497933216	1.19728277513057	3.16493991356996
H	5.08632083455057	1.76136848802302	1.62765982294522
C	7.58366611053974	2.56939236789123	2.04095229599588
H	8.59743768660885	2.70621248732490	1.64813103594031
H	7.59390166277574	2.60294645802595	3.14182052425951
H	6.93748270711994	3.36517878107150	1.64285981335688
C	6.64790706476600	-1.64587145794885	-1.70979812483770
H	7.14806509722943	-2.18055353040274	-0.89278958277866
H	7.15942961223852	-1.84664287573950	-2.66435532205642
H	5.59216812057380	-1.95115546008760	-1.75856507277939
C	4.36069970680566	2.82163607570336	-1.00288123721798
H	3.98304884558788	3.20305440127265	-0.04608484477271
H	3.72031738042752	3.19099612587963	-1.81948439452224
H	5.40351306776757	3.13688457189061	-1.15355097823860
C	3.45373761080967	-1.73310682887760	2.17123055496050
H	2.36192780953904	-1.64780483174086	2.24825965929386
H	3.86927099875721	-2.02889411844408	3.14686273916225

H	3.71738923850300	-2.46864836350450	1.39713910099187

Table S3: Geometry optimized coordinates of the dimer of [Ni^{II}(bmsab)dme] (**2**)

C	-2.41153260405356	-1.56912438633710	-0.45277335909900
C	-1.44947137420889	-2.57803335981877	-0.41444961860252
C	-0.28065164152776	-2.39264788197286	0.32549551052697
C	-0.04483030505014	-1.19903299304718	1.01184600520192
C	-1.04970891024789	-0.19378520966813	1.00343972252671
C	-2.22368328506621	-0.38901227217491	0.26443698165884
N	-0.79020514712642	0.88505353127155	1.82571049814743
N	1.16292141391144	-1.00084854630877	1.75502459503339
S	-1.04769878505435	2.44826335837773	1.60526645293588
S	2.37830201761216	-0.33859436111325	0.93350750650956
O	2.11366386673913	1.15989552600689	0.91571427855176
O	3.67497654181682	-0.70201795583891	1.50269715629093
O	-0.00646366841998	2.99792892912958	2.54893799159446
O	-2.41916283062264	2.91108623916944	1.77866528206369
C	-0.52859716485310	2.90793749800774	-0.03584833185692
H	0.51159780303574	2.58270199233792	-0.16373722761809
H	-1.19857200146862	2.42493470561289	-0.75914218499921
H	-0.62761580365158	3.99940550081624	-0.09611917716932
C	2.38506647333566	-0.82484593327934	-0.77924251230232
H	3.20525932178801	-0.25082488590967	-1.22912113582328
H	2.59348558647450	-1.89996672262790	-0.83331040087975
H	1.42479309411565	-0.58096974585909	-1.24753716033261
Ni	0.95433872833217	0.99814051272680	2.70467891029761
Ni	1.84530121671680	-1.68941617946164	7.80438021981633
N	2.45756000397915	-1.00783143334707	9.74718737054579
N	0.64040938619024	-2.97095870277441	8.92615520692147
C	0.78577697064341	-2.70476350163611	10.30467257608697
C	1.69730483357278	-1.70268819956313	10.71918843819232
C	1.86703125485077	-1.46322360979426	12.08906510851616
C	0.03483137470484	-3.38636344704467	11.27071816344425
C	0.19972244613345	-3.12079377846247	12.62822741766560
C	1.12427381761392	-2.16093209593032	13.03916220584939
S	1.42127957982514	-4.24974719216434	8.32190471635309
S	1.96089776698822	0.46188576136712	9.33124312193903
O	3.07314202750215	1.35841641543844	9.02914238754538
O	1.01410795318692	0.23251770350216	8.15696830844904
O	0.58903435082267	-5.09486699924007	7.47333450231418
O	2.61759176534448	-3.62878338126440	7.61451731227159
C	0.95171781065534	1.23520246230612	10.57725136401232
H	1.57394494339891	1.45508115549082	11.45231682470127
H	0.60546001460464	2.16619444326993	10.11012890759700
H	0.10897867753288	0.58402704213020	10.83619555969878
C	2.12107867339298	-5.27340850075970	9.60037683991074
H	1.31191520760887	-5.76690299974250	10.15077998426117
H	2.72398381824366	-6.01169166829298	9.05593824923727
H	2.74468343025618	-4.66541922368584	10.26601753769605
H	1.27228532185880	-1.95645893219895	14.10226431362266
H	-0.39559906246174	-3.66479392910269	13.36557894876154
H	-0.69577735120463	-4.12564089497457	10.93208633135440
H	2.61212215575493	-0.72648441941887	12.39980228237365
H	-2.99288959901541	0.38735175615616	0.28247472197809
H	-3.33082323498282	-1.71047919953640	-1.02668576912279
H	-1.61034219712005	-3.51462111404897	-0.95317666891915
H	0.47784731113686	-3.17849866212615	0.37380806298465
O	2.70215015626574	1.28680134159278	3.81170131826375
O	0.09629862683883	0.54333226867521	4.59593545502371
O	0.84476332345982	-1.91086193433305	5.95116270371907

O	3.42863601741664	-0.80189884934440	6.71155096411310
C	-0.75318740425191	-0.59854447769621	4.65499678765783
C	-0.49626580742574	-1.44153904676831	5.88605138268570
H	-1.81157888978446	-0.28717447751395	4.62894730290768
H	-0.56230861349847	-1.17155117284486	3.73801753972748
H	-0.65501445071370	-0.86256298889643	6.80563009165638
H	-1.19450042870373	-2.29752499701648	5.89770412220169
C	3.22313192416625	0.15026994307754	4.50815079297047
C	3.23872860536113	0.42204711478838	6.00127757506873
H	2.54913344790726	-0.69040074586138	4.30644840077944
H	4.20832991405527	-0.11327411723460	4.09456809045406
H	4.01160463006407	1.14584297010914	6.30246275309181
H	2.26825414751498	0.82969216794383	6.30718135495679
C	4.74362379944648	-1.01262333882591	7.21203440272617
H	4.75685648238666	-2.01590498300291	7.65566219947945
H	5.47679760984541	-0.96776290100410	6.39046302360583
H	4.97969611452955	-0.26157215759323	7.98172099930291
C	1.15577844132776	-2.95522422189299	5.02672457536483
H	2.19120521331501	-3.25109519239290	5.22493096657049
H	0.50459645612563	-3.82434681978645	5.20734610423545
H	1.06304623970056	-2.59699138159747	3.98964048834178
C	-0.35826033477558	1.65062473665268	5.36950677525989
H	0.37925057189448	2.45188418609938	5.24536344955538
H	-1.33066451216956	2.00495672102360	4.99204078518407
H	-0.41753289659283	1.37583873491320	6.43303729978493
C	3.69372424973093	2.18449907080729	3.32236058286495
H	3.16658782498299	3.03951060921793	2.88172391194458
H	4.32930443968630	2.53430613549672	4.15115941652469
H	4.30058310834947	1.69032558861675	2.54958405526095

Table S4: Geometry optimized coordinates of a monomer of [Co^{II}(bmsab)dme] (**3**)

C	-2.19151332888963	1.54502478055777	-0.76951699494450
C	-2.11560572225804	0.37404699208314	-1.51783096963480
C	-0.93977282574000	-0.38063199219201	-1.53123491102012
C	0.15770490825229	0.02139757817011	-0.76814502279532
C	0.07890846639089	1.21997257600586	-0.00299520176916
C	-1.09250936193602	1.97800706214016	-0.02382934473963
N	1.25971510286133	1.51872448233941	0.68040979262480
N	1.39666767915459	-0.62101017528714	-0.67081878471816
S	1.56213965382915	2.80367437016868	1.60966594206090
S	1.80716410536431	-2.02817558856260	-1.35624094593096
O	3.22342420087157	-2.19980921215948	-0.96486118702991
O	1.45483470800917	-2.13328186187655	-2.76902635842285
O	3.00159018614659	2.65664061645316	1.92641736728799
O	1.09958872703541	4.07377526953002	1.05516052500207
C	0.68265041633267	2.56081546286745	3.14345421003667
H	1.04689402274802	1.64336671696346	3.62002324188797
H	-0.39255911484424	2.49755067075780	2.93153039759837
H	0.89863697452223	3.43897558012330	3.76578907817116
C	0.88127863532502	-3.30169124951764	-0.50959940066481
H	1.15090429704992	-4.25125408798880	-0.98977610055924
H	-0.19096242991350	-3.10303640585810	-0.63544603478196
H	1.15522119722905	-3.30535926176922	0.55188022778349
Co	2.75892684730556	0.35025842261651	0.29835060317680
H	-1.12726069214234	2.92690413847056	0.51471631582195
H	-3.10416800971954	2.14556372844355	-0.77780699678231
H	-2.96750586719577	0.04927742122371	-2.11980500029516
H	-0.85622358470969	-1.26350759615999	-2.16779140699939
O	4.09159711804263	-0.58894350692586	1.61082823518099
O	4.52620393106247	1.20149619433527	-0.36880127933417
C	5.41053873987273	-0.41591066789432	1.09616956125700
C	5.52532076929153	1.01084158621825	0.62825343080781
H	5.57348633997946	-1.12121839692460	0.26291707731904
H	6.14725478633303	-0.61210486479247	1.89365063095556
C	4.49051277562548	2.52194146765533	-0.91370343632217
H	4.21429889300810	3.24540813741713	-0.13251032862800
H	3.72783917340321	2.51881378782238	-1.70217041602418
H	5.47130190235317	2.76457421286937	-1.35207218480673
C	3.83990095052100	-1.90056487807503	2.10488952951051
H	2.83194119112543	-1.88871851910953	2.53911243475090
H	4.57072656022420	-2.14714232285183	2.89172227669593
H	3.88319074047076	-2.62906013746079	1.28135733642837
H	6.52350912668518	1.18444653683397	0.19153434636185
H	5.35276781092229	1.71623293333955	1.45859974548331

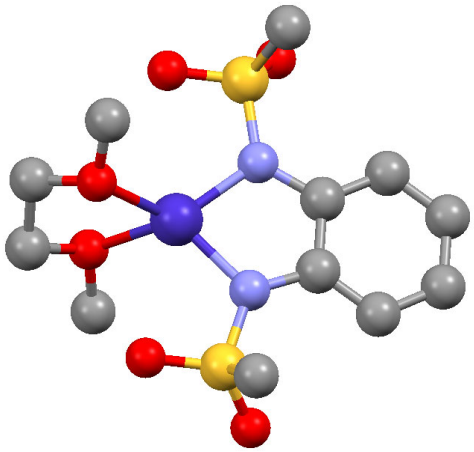

Figure S17: Theoretical structure of the monomeric version of **[Co^{II}(bmsab)dme]** (**3**). The geometry was optimized on the DFT level as described in the methods section. Oxygen is shown in red, nitrogen in light blue, carbon in grey, sulphur in yellow and cobalt in dark blue. Hydrogens are omitted for clarity.

Table S5: Geometry optimized coordinates of a monomer of [Ni^{II}(bmsab)dme] (**2**)

C	-2.12984541227537	1.66147748067818	-0.67324192384354
C	-2.15790885222230	0.49633374681991	-1.43602418164405
C	-1.01764492247316	-0.30314125652167	-1.52732349299228
C	0.13444317847929	0.05631192400950	-0.82963909317531
C	0.17575351352567	1.24783929065300	-0.05266575323563
C	-0.97107447765635	2.04805582256844	0.00381505761442
N	1.41327631363942	1.48341468528358	0.55564568603678
N	1.34450385416381	-0.62517987104299	-0.80524697618916
S	1.67441170264651	2.70274747410769	1.59159840380800
S	1.77084653226392	-2.03428361331264	-1.46410480166600
O	3.18887527202903	-2.13535059983552	-1.02818235314463
O	1.45396489094959	-2.17910758116830	-2.87896393328867
O	3.10685021788850	2.62993332063226	1.92912953558479
O	1.14950829134064	3.98448645770398	1.12081878092020
C	0.78652706132857	2.30253458882889	3.09023670896369
H	1.19907044978299	1.37648031048001	3.50756388044154
H	-0.28077267190638	2.19246320427397	2.85805000712790
H	0.94408105245141	3.14502586826155	3.77625979000271
C	0.87464505108284	-3.31594567505241	-0.60300831680767
H	1.19584112039648	-4.26771705425180	-1.04594781851104
H	-0.20034857924972	-3.16453917236287	-0.76524822057649
H	1.11968595047535	-3.27566641138077	0.46463711958138
Ni	2.79622390320207	0.14516810632813	0.10767654777504
H	-0.94023904362095	2.99432461640257	0.54557772624874
H	-3.01500936414760	2.29971202271324	-0.61687998605814
H	-3.06135560159601	0.21479548842670	-1.98160783907254
H	-1.00509323009623	-1.18996598673576	-2.16499480509851
O	4.03239515396560	-0.50493266785312	1.65803519150110
O	4.53143124380023	1.11920225265342	-0.38701950824789
C	5.39167376947838	-0.26609986268394	1.30153223840188
C	5.45228654068376	1.11142884954304	0.70149666231455
H	5.72105001253480	-1.03156613458706	0.57707104694780

H	6.02731042886321	-0.32004133554983	2.20162384762265
C	4.40598909609990	2.39382915755207	-1.02057322254822
H	4.02139643326295	3.13356633078433	-0.30379669200028
H	3.69715020134237	2.27071884434735	-1.84823773584008
H	5.38639510993647	2.70239690151997	-1.41680570754520
C	3.80209288865301	-1.80983191662681	2.17306303567640
H	2.75169883078704	-1.84881602486925	2.48920649216687
H	4.44889755929292	-1.98632188344348	3.04752513539977
H	3.98354368735200	-2.57009819635445	1.39712568900596
H	6.46967811602823	1.31965774168801	0.32887359096857
H	5.14635472751677	1.87301075737280	1.43540018737453

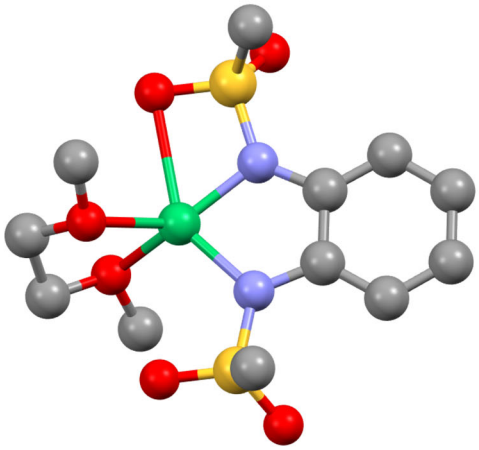

Figure S18: Theoretical structure of the monomeric version of **[Ni^{II}(bmsab)dme]** (**2**). The geometry was optimized on the DFT level as described in the methods section. Oxygen is shown in red, nitrogen in light blue, carbon in grey, sulphur in yellow and nickel in green. Hydrogens are omitted for clarity.

Table S6: Comparison of the relevant bond length of the calculated structure of **3** to the experimental structure of the corresponding homoleptic complex.[1,2]

Bond	**3** Center 1	**3** Center 2	[Co(II)(bmsab)$_2$(K-18-c-6)$_2$ Ligand 1	Co(II)(bmsab)$_2$(K-18-c-6)$_2$ Ligand 2	Co(II)(bmsab)$_2$(HNEt$_3$)$_2$ Ligand 1	Co(II)(bmsab)$_2$(HNEt$_3$)$_2$ Ligand 2
Co-N1	1.967	1.942	2.005	2.026	2.004	1.998
Co-N2	1.946	1.969	2.008	1.995	2.010	2.013
C-N1	1.401	1.396	1.418	1.415	1.414	1.409
C-N2	1.397	1.401	1.411	1.410	1.418	1.415

Table S7: Individual contributions to the *D*-tensor for **3**, Co(II)-center 1. Calculations were carried out on CASSCF/NEVPT2 level, with a def2-TZVPP basis set for the metal center and the first coordination sphere.

Mult	Root	D	E
4	1	-54.207	0.059
4	2	7.849	1.286
4	3	2.964	1.741
4	4	5.887	-3.195
4	5	0.258	0.154
4	6	0.095	0.035
4	7	0.004	0.002
4	8	0.008	0.001
4	9	0.006	-0.002
2	0	-0.134	0.362
2	1	0.551	0.206
2	2	-0.025	0.019
2	3	-0.291	-0.232
2	4	0.151	-0.017
2	5	0.369	0.005
2	6	5.836	-0.013
2	7	-3.082	-1.893
2	8	-1.521	1.043

Table S8: Individual contributions to the *D*-tensor for **3**, Co(II)-center 2. Calculations were carried out in accordance with Co(II)-center 1 on a CASSCF/NEVPT2 level. Again, a def2-TZVPP basis set for the metal center and the first coordination sphere was used.

Mult	Root	D	E
4	1	-50.614	0.071
4	2	7.768	-5.177
4	3	4.063	4.217
4	4	5.858	-0.021
4	5	0.040	-0.000
4	6	0.165	0.112
4	7	0.002	-0.002
4	8	0.011	0.004
4	9	0.009	-0.002
2	0	1.101	-0.012
2	1	-0.706	0.210
2	2	-0.006	0.009
2	3	-0.107	-0.046
2	4	-0.050	-0.015
2	5	0.454	-0.002
2	6	5.944	-0.012
2	7	-3.352	-0.288
2	8	-1.559	0.014
2	9	-0.008	-0.009

Table S9: Individual contributions to the *D*-tensor for **2**, Ni(II)-center 1. As for the previous two tables, calculations were carried out on CASSCF/NEVPT2 level with a def2-TZVPP basis set for the metal center and the first coordination sphere.

Mult	Root	D	E
3	1	-58.659	-0.660
3	2	21.817	-21.600
3	3	19.870	18.539
3	4	0.779	-0.077
3	5	0.710	-0.521
3	6	0.321	0.346
3	7	0.044	0.039
3	8	0.042	-0.012
3	9	-0.003	0.001
1	0	0.082	0.004
1	1	0.006	-0.000
1	2	16.237	0.020
1	3	-6.883	6.903
1	4	-6.695	-6.650
1	5	-0.424	0.204
1	6	-0.012	0.013
1	7	-0.178	0.101
1	8	-0.019	-0.018
1	9	-0.029	0.002

Table S10: Individual contributions to the *D*-tensor for **2**, Ni(II)-center 2. As for center 1, calculations were carried out again on CASSCF/NEVPT2 level with a def2-TZVPP basis set for the metal center and the first coordination sphere.

Mult	Root	D	E
3	1	-38.184	-4.178
3	2	14.264	-8.020
3	3	12.677	11.591
3	4	0.110	-0.166
3	5	-0.052	-0.009
3	6	0.006	-0.001
3	7	0.000	0.000
3	8	0.001	-0.002
3	9	-0.003	-0.000
1	0	0.005	-0.006
1	1	0.004	-0.001
1	2	15.691	0.033
1	3	-7.012	7.063
1	4	-7.122	-7.125
1	5	-0.005	-0.001
1	6	-0.227	0.180
1	7	-0.092	0.064
1	8	-0.125	-0.115
1	9	-0.139	-0.044

Sample Inputs for ORCA Calculations

Sample input for a CASSCF calculation, used for the calculation of the spin Hamiltonian parameters for **2** and **3** as well as for the monomeric structures.

```
! def2-TZVP autoaux PATOM Normalprint RI-NEVPT2
! tightscf slowconv
! MORead
%moinp "desiredfilefrompreviouscalc.gbw"
%pal
 nprocs 20
end
%scf
MaxIter 500
end
%maxcore 15000
%casscf
nel 7 or 8
norb 5
mult 4,2 or 3,1
nroots 10,10 or 10,9
Trafostep ri
rel
dosoc true
gtensor true
dtensor true
end
end

%coords
CTyp xyz
Charge 0
Mult 4 or 3
Units Angs
Coords
      Coordinates of each molecule. One center is exchanged for Zn instead
      of Co or Ni. Here the
          newgto "def2-TZVPP" end
          newauxgto "def2/J" end
      keywords were used for the atoms, where different basis sets were
      needed
end
end
```

Sample input for the broken symmetry DFT calculations used in this work

```
! PBE0 def2-SVP def2/J
! RIJCOSX

%pal
 nprocs 10
end
%scf
Flipspin 0
FinalMs 0.0
MaxIter 1000
end

%maxcore 15000

%coords
CTyp xyz
Charge 0
Mult 7 or 5
Units Angs
Coords
      Coordinates of each molecule. Metal centers have to be in first
      positions of the coordinates. Here also the
          newgto "def2-TZVPP" end
          newauxgto "def2/J" end
      keywords were used for the atoms, where different basis sets were
      needed
end
end
```

Analytic for the Complexation Experiments – Compounds **4**a and **4**b

NMR Spectra

Zn(bmsab)DTBBPy

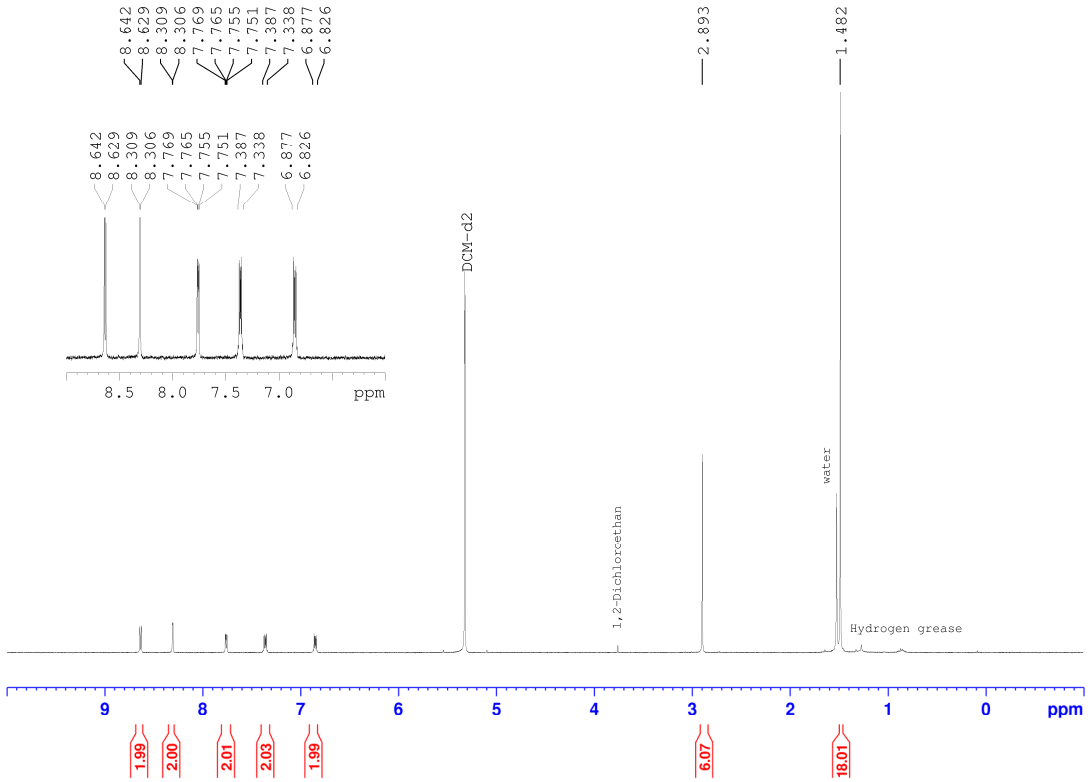

Figure S19: [1]H-NMR-Spectrum (400 MHz, DCM-*d2*, 25 °C) of the heteroleptic Zn(II) complex **Zn(bmsab)DTBBPy 4**a dissolved in deutero-dichloromethane.

Mass Spectrometry

Zn(bmsab)DTBBPy

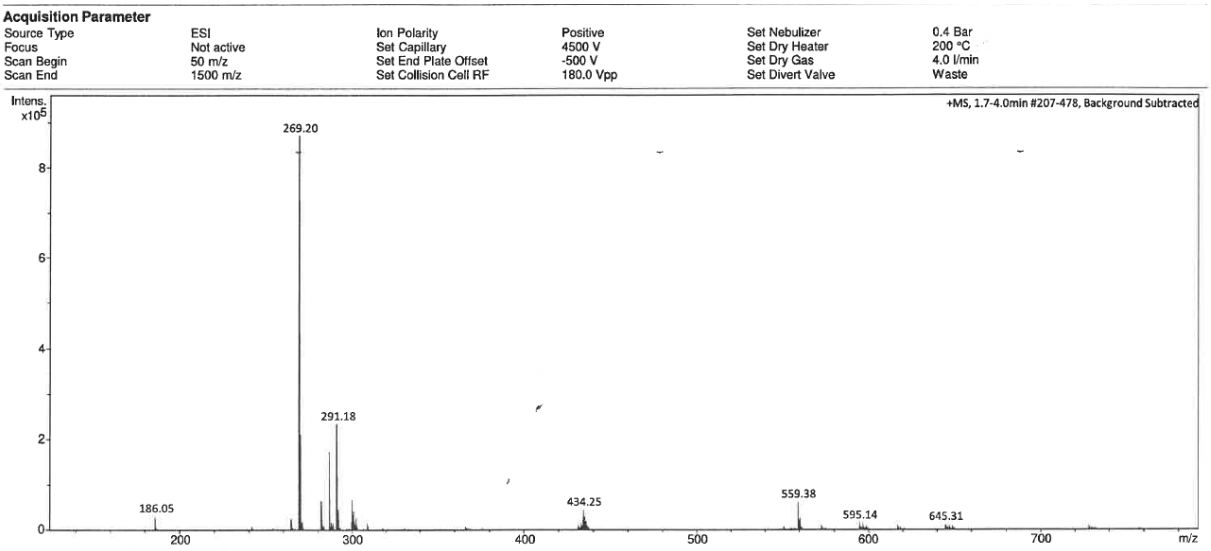

Figure S20: ESI(+)-Mass-spectrum of **Zn(bmsab)DTBBPy 4**a measured on a Bruker micrOTOF-Q

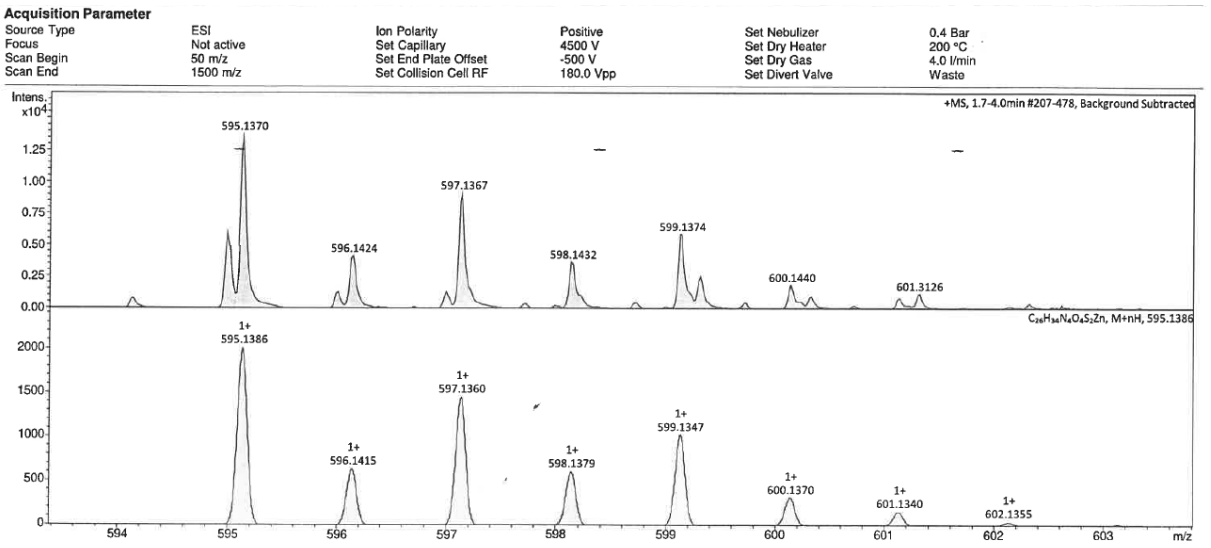

Figure S21: ESI(+)-mass-spectrum of the molecular ion of **Zn(bmsab)DTBBPy 4**a (top) with calculated isotope pattern (bottom).

Co(bmsab)DTBBPy

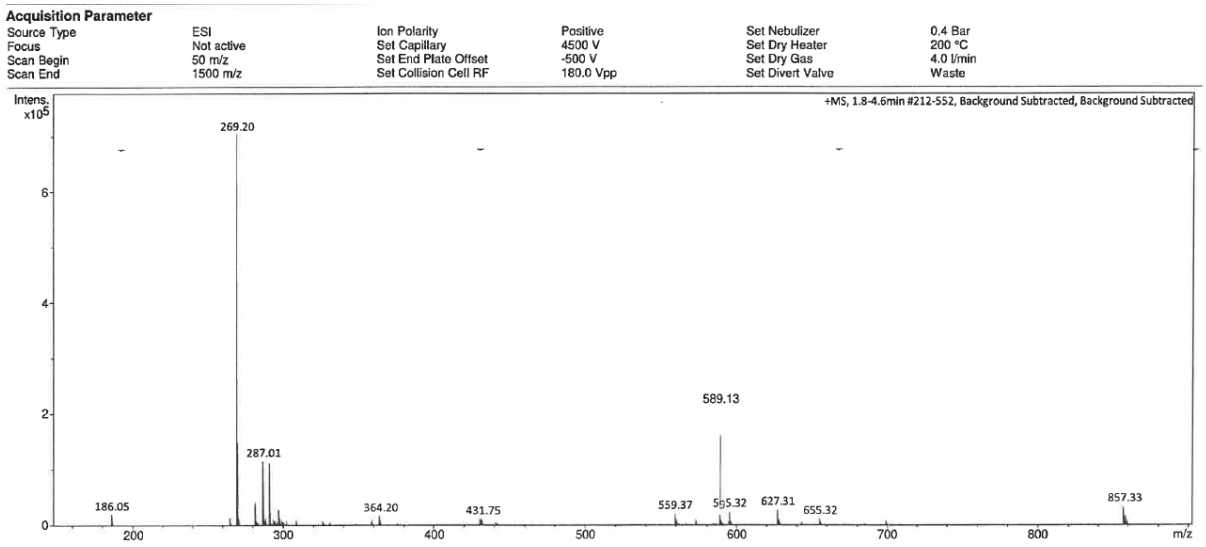

Figure S22: ESI(+)-Mass-spectrum of **Co(bmsab)DTBBPy 4**b measured on a Bruker micrOTOF-Q.

References

(1) Bamberger, H.; Albold, U.; Dubnická Midlíková, J.; Su, C.-Y.; Deibel, N.; Hunger, D.; Hallmen, P. P.; Neugebauer, P.; Beerhues, J.; Demeshko, S. *et al.* Iron(II), Cobalt(II), and Nickel(II) Complexes of Bis(sulfonamido)benzenes: Redox Properties, Large Zero-Field Splittings, and Single-Ion Magnets. *Inorg. Chem.* **2021**, *60*, 2953–2963.

(2) Rechkemmer, Y.; Breitgoff, F. D.; van der Meer, M.; Atanasov, M.; Hakl, M.; Orlita, M.; Neugebauer, P.; Neese, F.; Sarkar, B.; van Slageren, J. A four-coordinate cobalt(II) single-ion magnet with coercivity and a very high energy barrier. *Nat. Commun.* **2016**, *7*, 268.

(3) Bain, G. A.; Berry, J. F. Diamagnetic Corrections and Pascal's Constants. *J. Chem. Educ.* **2008**, *85*, 532.